MODULATION OF GLIOBLASTOMA CELL BEHAVIOR BY MONOCYTE-DERIVED MACROPHAGES AND FREQUENCY-DEPENDENT ATTRACTION ON A MICROFLUIDIC CHIP

by
HANİFE KANTARCI

Submitted to the Graduate School of Engineering and Natural Sciences
in partial fulfilment of
the requirements for the degree of Master of Science

Sabancı University
July 2025

ABSTRACT

MODULATION OF GLIOBLASTOMA CELL BEHAVIOR BY MONOCYTE-DERIVED MACROPHAGES AND FREQUENCY-DEPENDENT ATTRACTION ON A MICROFLUIDIC CHIP

HANİFE KANTARCI

Molecular Biology, Genetics and Bioengineering M.Sc. Thesis, July 2025

Thesis Supervisor: Assoc. Prof. Meltem Elitaş

Keywords: glioblastoma multiforme, tumor microenvironment, monocyte-derived macrophages, glioma cell behavior, dielectrophoresis, microfluidic chip

Glioblastoma Multiforme (GBM) is a highly aggressive and heterogeneous primary brain tumor, marked by rapid proliferation, therapeutic resistance, and complex interactions within the tumor microenvironment (TME). Among the key modulators of the TME are tumor-associated macrophages (TAMs), which play a pivotal role in shaping glioma behavior and influencing treatment outcomes. This thesis investigates the impact of monocyte-derived macrophage phenotypes (M0, M1, and M2) on glioma cell proliferation and migration. THP-1 cells were differentiated into macrophage subtypes via cytokine-driven protocols. Functional assays revealed that M1 macrophages enhanced glioma proliferation while attenuating migratory capacity, whereas M2 macrophages initially suppressed proliferation, followed by increased growth and significantly enhanced wound closure, suggesting a dual-phase modulatory effect.

To enable precise, label-free cellular analysis, a microfluidic platform incorporating dielectrophoresis (DEP) was developed. Computational simulations validated optimal electric field distributions for effective DEP-based manipulation of glioma cells. The DEP buffer was shown to preserve glioma cell viability, supporting its potential use in non-destructive diagnostics. Additionally, impedance spectroscopy confirmed the system's sensitivity to cellular heterogeneity across different glioma lines. Device performance was validated using U-87 glioma cells, demonstrating reliable cell

behavior tracking and morphological assessment.

Overall, the study underscores the regulatory role of macrophage subtypes in GBM progression and highlights the promise of DEP-integrated microfluidics for advanced glioma diagnostics and future therapeutic applications.

ÖZET

GLIOBLASTOMA HÜCRE DAVRANIŞININ MONOSIT KÖKENLI MAKROFAJLAR TARAFINDAN DÜZENLENMESI VE MIKROAKIŞKAN ÇIP ÜZERINDE FREKANSA BAĞIMLI ÇEKIM

HANİFE KANTARCI

Moleküler Biyoloji, Genetik ve Biyomühendislik Yüksek Lisans Tezi, Temmuz 2025

Tez Danışmanı: Doç. Dr. Meltem Elitaş

Anahtar Kelimeler: glioblastom, tümör mikroçevresi, monosit kökenli makrofajlar, glioma hücre davranışı, dielektroforez, mikroakışkan çip

Glioblastom, hızlı proliferasyon, tedaviye direnç ve tümör mikroçevresi (TME) içindeki karmaşık etkileşimlerle karakterize edilen, son derece agresif ve heterojen bir primer beyin tümörüdür. TME'nin temel düzenleyicileri arasında, glioma hücrelerinin davranışını şekillendiren ve tedavi sonuçlarını doğrudan etkileyen tümörle ilişkili makrofajlar (TAM'lar) yer almaktadır. Bu tezde, monosit kaynaklı makrofaj fenotiplerinin (M0, M1 ve M2) glioma hücre proliferasyonu ve migrasyonu üzerindeki etkileri araştırılmıştır. THP-1 hücreleri, sitokin aracılı protokoller ile farklı makrofaj alt tiplerine farklılaştırılmıştır. Fonksiyonel analizler sonucunda, M1 makrofajlarının glioma proliferasyonunu artırdığı ancak hücresel migrasyonu azalttığı; M2 makrofajlarının ise başlangıçta proliferasyonu baskıladığı, ardından büyümeyi artırdığı ve yara kapanmasını belirgin şekilde hızlandırdığı görülmüş, böylece iki aşamalı düzenleyici bir etki ortaya koyduğu belirlenmiştir.

Hassas ve etiket gerektirmeyen hücre analizini mümkün kılmak amacıyla, dielektroforez (DEP) temelli bir mikroakışkan platform geliştirilmiştir. Hesaplamalı simülasyonlar, glioma hücrelerinin DEP aracılığıyla etkin biçimde manipülasyonu için optimal elektrik alan dağılımlarını doğrulamıştır. DEP tamponunun hücre canlılığını koruduğu gösterilmiş, bu durum yöntemin yıkıcı olmayan tanısal uygulamalarda kullanılabilirliğini desteklemiştir. Ayrıca, empedans spektroskopisi, farklı glioma hücre hatları arasındaki heterojenliği ayırt etme duyarlılığını doğrulamıştır.

Cihazın performansı, U-87 glioma hücreleri ile yapılan deneylerde test edilmiş ve güvenilir hücre davranışı takibi ile morfolojik değerlendirmeler sağlanmıştır.

Sonuç olarak, bu çalışma, makrofaj alt tiplerinin GBM progresyonundaki düzenleyici rollerini ortaya koymakta ve DEP entegre mikroakışkan sistemlerin gelişmiş glioma tanısı ile gelecekteki terapötik uygulamalar için güçlü bir potansiyele sahip olduğunu göstermektedir.

ACKNOWLEDGEMENTS

First of all, I would like to express my gratitude to myself. My self-confidence and belief have carried me through this journey. Yet, I could not have stood strong without my family who never doubted me.

I want to thank my advisor, Assoc. Prof. Meltem Elitaş, for offering me a position in her lab and a multidisciplinary project that expanded my knowledge in combining biology with engineering aspects. I also would like to thank Prof. Betül Yılmaz, Assoc. Prof. Ali Fuat Ergenç and Assoc. Prof. Murat Kaya Yapıcı for their valuable support of the project. I want to thank my jury member Assoc. Prof. Özlem Kutlu for her evaluation and insightful suggestions for future direction of this work.

There is special thanks to the Scientific and Technological Research Council of Turkey (TÜBİTAK) for financial support to our project under grant number 222Z005. I gratefully acknowledge the Faculty of Natural Sciences and Engineering at Sabancı University, and Sabancı University Nanotechnology Research and Applications Center (SUNUM) for their technical assistance and equipment support.

I would like to express my appreciation to Andisheh Choupani for designing and fabricating our chip and collaborating with me on microscopic analysis. I also thank Negar Amirhaghian for her help in impedance spectrometry. My labmate and close friend, Miray Esra Palaz provided invaluable support during the challenging thesis process. I want to thank Buğra Şenel who was always willing to answer my questions patiently. I want to extend my thanks to many other colleagues in my university, who are always willing to help and guide me without asking for any help. When I started this journey, my knowledge of cell culture and microfluidic systems was very limited, and it was significantly shaped with the support of laboratory technicians and my friends, particularly Ramazan, Ünal, and İsmail, who patiently answered my persistent questions.

I believe that I have built strong and lasting friendships during my time at Sabancı University. These friendships have created a lovely and liveable place with strong respect for me. I cannot define my feelings and give all names here, but I would like to mention Buğra, Ceren, Miray, Mustafa Kemal, Armita, Elif, Rabia, Gülce, Esma, Feyza, Merve, Kübranur, Büşra, Mustafa...

My deepest thanks go to my family; my mother Emine, my father Musa, my brother

Davut and my sister Bahar. I am also thankful to my siblings for the joy brought into my life by my lovely niece Zeynep Alya and nephew Alparslan, who blossom flowers in my heart. Their courage and presence have been my strongest source of strength.

TABLE OF CONTENTS

LIST OF TABLES

LIST OF FIGURES

LIST OF SYMBOLS AND ABBREVIATIONS

ε_m Permittivity of medium

ε_p Permittivity of particle

E Electric field

F_{DEP} Dielectrophoretic force

$K(\varepsilon_p, \omega)$ Clausius–Mossotti factor

R Radius of particle

Z'' Imaginary component of impedance

Z' Real component of impedance

AC Alternating Current

ARG1 Arginase-1

CCK-8 Cell Counting Kit-8

CD11b Cluster of Differentiation 11b

CD14 Cluster of Differentiation 14

CM Conditioned Medium

CNS Central Nervous System

CO_2 Carbon Dioxide

DEP Dielectrophoresis

DMEM Dulbecco's Modified Eagle Medium

DMSO Dimethyl Sulfoxide

ECM Extracellular Matrix

EGF Epidermal Growth Factor

ELISA Enzyme-Linked Immunosorbent Assay

EMT Epithelial–Mesenchymal Transition

FACS Fluorescence-Activated Cell Sorting

FBS Fetal Bovine Serum

GAM Glioma-Associated Myeloid Cell

GBM Glioblastoma Multiforme

HGF Hepatocyte Growth Factor

LPS Lipopolysaccharide

M-CSF Macrophage Colony-Stimulating Factor

MACS Magnetic-Activated Cell Sorting

MDM Monocyte-Derived Macrophages

MMP Matrix Metalloproteinase

MRI Magnetic Resonance Imaging

nDEP Negative Dielectrophoresis

NK Natural Killer cells

PBS Phosphate Buffered Saline

PD-L1 Programmed Death-Ligand 1

pDEP Positive Dielectrophoresis

PET Positron Emission Tomography

PI Propidium Iodide

PMA Phorbol 12-Myristate 13-Acetate

rhIFN-γ Recombinant Human Interferon-Gamma

rhIL-13 Recombinant Human Interleukin-13

rhIL-4 Recombinant Human Interleukin-4

RPMI 1640 Roswell Park Memorial Institute Medium 1640

SEM Scanning Electron Microscope

TAM Tumor-Associated Macrophage

TGF-β Transforming Growth Factor-beta

TME Tumor Microenvironment

TNF-α Tumor Necrosis Factor-alpha

Tregs Regulatory T cells

VEGF Vascular Endothelial Growth Factor

1. INTRODUCTION

1.1 Glioblastoma

Glioblastoma multiforme (GBM) is one of the most aggressive and common brain tumors which is classified as IV grade glioma. High proliferation rate, ability to invade surrounding brain tissues, possessing resistance to conventional therapies, extensive vascularization (angiogenesis), immunosuppression and necrosis are the characteristics of GBM (Louis et al., 2021). The progression of GBM has four stages ranging from lower-grade (grades I-II) to highly malignant (grades III-IV). The survival rate of patients is nearly 15 months and unfortunately, only %5 percent of patients can continue their life for 5 years after diagnosis. Its prognosis is very poor, however the advancement in neuro-oncology. Current ways like tumor resection, radiation therapy, and application of chemotherapy drugs are not enough for GBM. Even after surgical resection, it shows a high recurrence rate. Therefore, it is often referred as "a systemic whole-brain disease" instead of a tumor localized in the brain. This emphasizes the complex nature of GBM and dynamic communication within its microenvironment (Sisakht et al., 2022).

The heterogeneity of glioblastoma causes complications in its diagnosis, prognosis, and treatment, while it contributes to the aggressiveness of GBM and its resistance to therapeutics. It can exist on several levels. Genetic and molecular heterogeneity arises from the presence of mutations and molecular markers in each tumor. They can be driver mutations and amplifications like TP53 and IDH mutations, and epigenetic modifications like methylation at MGMT promoter. Additionally, gene expression patterns are utilized to classify GBM. They can be classified as classical (EGFR amplification), mesenchymal (NF1 mutations), and proneural (TP53 and IDH mutations) (Figure 1.1). In cellular heterogeneity, GBM possesses multiple cell types that function in tumor progression. These cells are generally cancer stem

cells, GBM differentiated cells, immune cells and vascular cells. These cell populations represent dynamic interaction and function in tumor resistance and progression (Zottel et al., 2023; Hegi et al., 2005). The other factor is the microenvironmental heterogeneity of GBM, which includes hypoxic conditions that trigger angiogenesis, an extracellular matrix that supports tumor invasion, and immune suppression that allows GBM cells to evade immune detection. Several heterogeneity levels form an adaptive tumor ecosystem, resulting in the failure of therapeutic approaches and increasing the importance of personalized treatment methods (Eisenbarth & Wang, 2023).

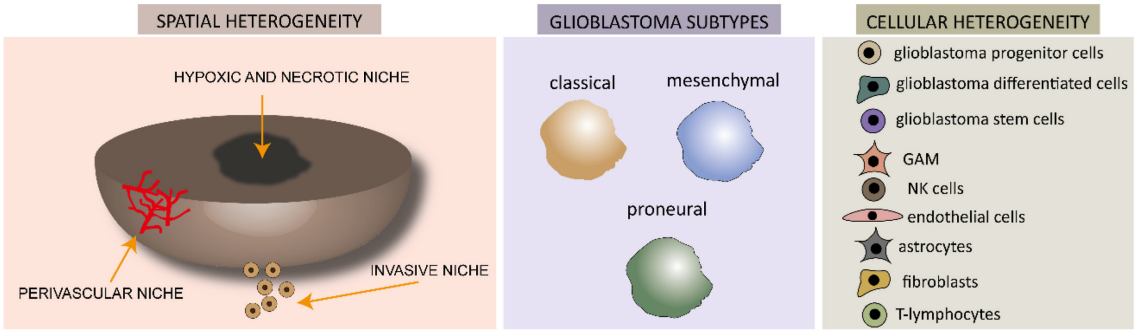

Figure 1.1 The representation of GBM heterogeneity (Zottel et al., 2023)

1.1.1 Tumor Microenvironment of GBM

Extracellular Matrix (ECM) is crucial for invasion, progression and therapeutic resistance of GBM. ECM is not just a scaffold for the tumor; it functions in signaling pathways and cell behavior. It consists of hyaluronic acid, which creates a hydrophilic environment, and functions in cell migration, as well as proteoglycans that facilitate both cell adhesion and invasion, along with collagens and laminins. Moreover, ECM can be remodeled during GBM progression. Matrix metalloproteinases (MMPs) degrade ECM components for invasion, while integrin signaling mediates cell-ECM adhesion and migration. These alterations in stiffness and mechanical properties of ECM influence tumor cell behaviour (Bellail et al., 2004; Marino et al., 2023).

The tumor microenvironment (TME) contains several cell types as non-cancerous and cancerous which are combined with ECM, chemokine/cytokine, growth factors and some specific conditions like hypoxia (Figure 1.2). Their difference in distribution within the glioma niche enables communication and crosstalk between them, which function in tumor angiogenesis, progression, growth, recurrence, and invasion.

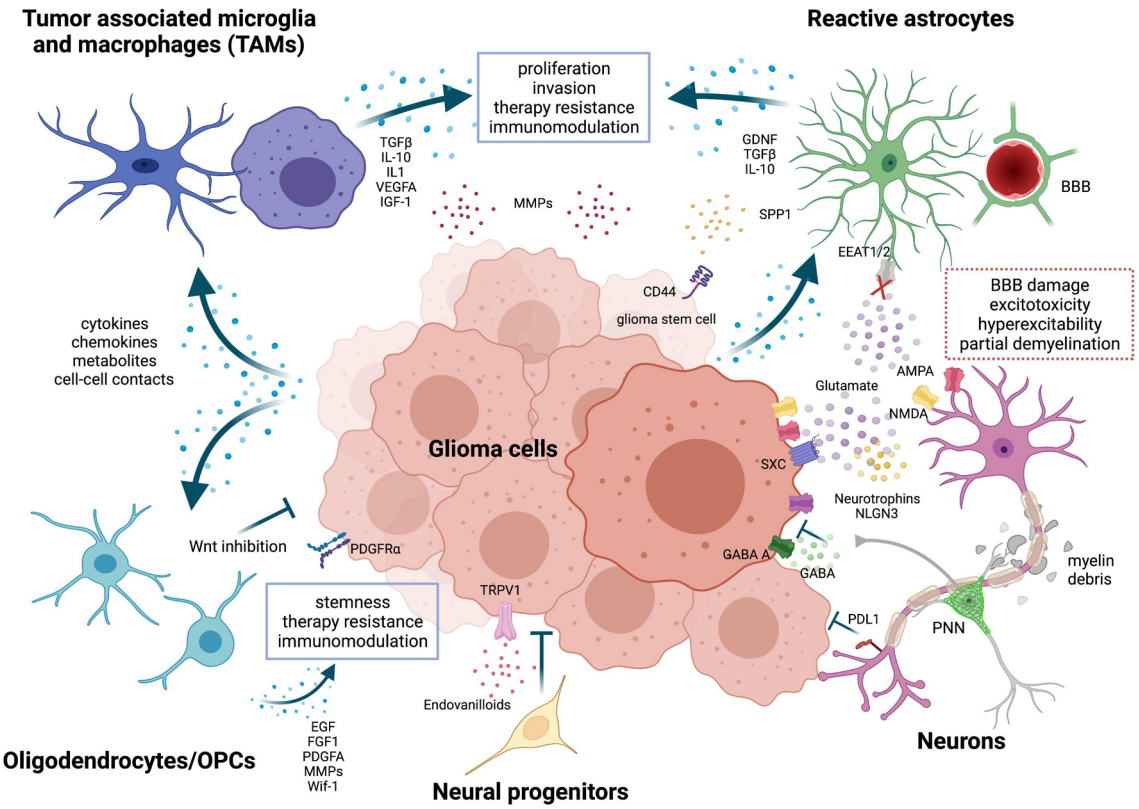

Figure 1.2 The representation of neurons and glial cells in tumor microenvironment (Parmigiani et al., 2021)

The main components of this microenvironment consist of ECM, growth factors, chemokines, cytokines and resident/infiltrating cells. One of the cell types in TME is the astrocyte that contributes to homeostasis, provides structural support, stores energy, organizes and remodels synapses, and protects against oxidative stress (Bikfalvi et al., 2022; Read et al., 2024). It is also essential for the formation of the blood-brain barrier. They cover nearly 99% of the brain surface. As another type, cancer stem cells, which are initiators of tumors due to their self-renewal ability, play a role in recurrence because of their powerful resistance to radiotherapy and chemotherapy (Sisakht et al., 2022). A remarkable feature of TME is infiltration of immune cells which involves nearly 30% of all tumor cells. These are T lymphocytes, natural killer (NK) cells, microglia, and macrophages derived from bone marrow (Erices et al., 2023).

1.2 Immune Cell Heterogeneity in GBM

Among the infiltration of several cellular compartments in the tumor microenvironment, immune cells show a complex and substantial population. The most prominent adaptive immune cells are tumor-infiltrating lymphocytes. $CD4^+$ helper T cells function in coordination of immune response via enhancing cytokine production. $CD8^+$ cytotoxic T cells directly function on elimination of tumor cells by antigen-specific degradation. The other subset of T lymphocytes is regulatory T cells (Tregs) that suppress excessive amounts of immune activation; however, they mostly contribute to immune evasion in tumor conditions. Additionally, $CD4^+$ helper T cells exhibit higher amount compare to $CD8^+$ cytotoxic T cells in aggressive GBM subtypes (Strepkos et al., 2019; Gieryng et al., 2017). On the other hand, NK cells possess a crucial inhibitory role in limiting the invasiveness of GBM and metastasis. Unfortunately, tumor cells upregulate immune checkpoint molecules to evade NK-mediated cytotoxicity (Lee et al., 2015).

Microglia are localized immune cells in the central nervous system (CNS). Their reprogramming into tumor-supporting cells enhances the progression and invasion of glioma. Its activation results in upregulation of metalloproteinases that trigger cell migration. Furthermore, the cross-talk between microglia and glioma involves Wnt/β-catenin signaling that promotes macrophage 2-like microglial phenotype as protumor function (Erices et al., 2023).

1.2.1 Origin and Spatial Distribution of TAMs

Tumor-associated macrophages (TAMs) in GBM arise from two different sources, bone marrow-derived monocytes and resident microglia (Figure 1.3). Microglia form during embryonic development and they are long-lived cells in the CNS. They function in immune surveillance, repair, and homeostasis. Compared to microglia, chemokine release in TME recruits bone marrow–derived monocytes into the environment when the integrity of the blood-brain barrier is altered in tumor progression. They are enriched in the perivascular region and tumor core, where high cytokine levels and hypoxic conditions support immune suppression. Microglia interacts with invading tumors due to its residence in the tumor margins. These differences are critical to understand their roles in tumor development and therapeutic response. There should be a separation of these populations in experimental models to distinguish (Khan et al., 2023; Chen et al., 2021).

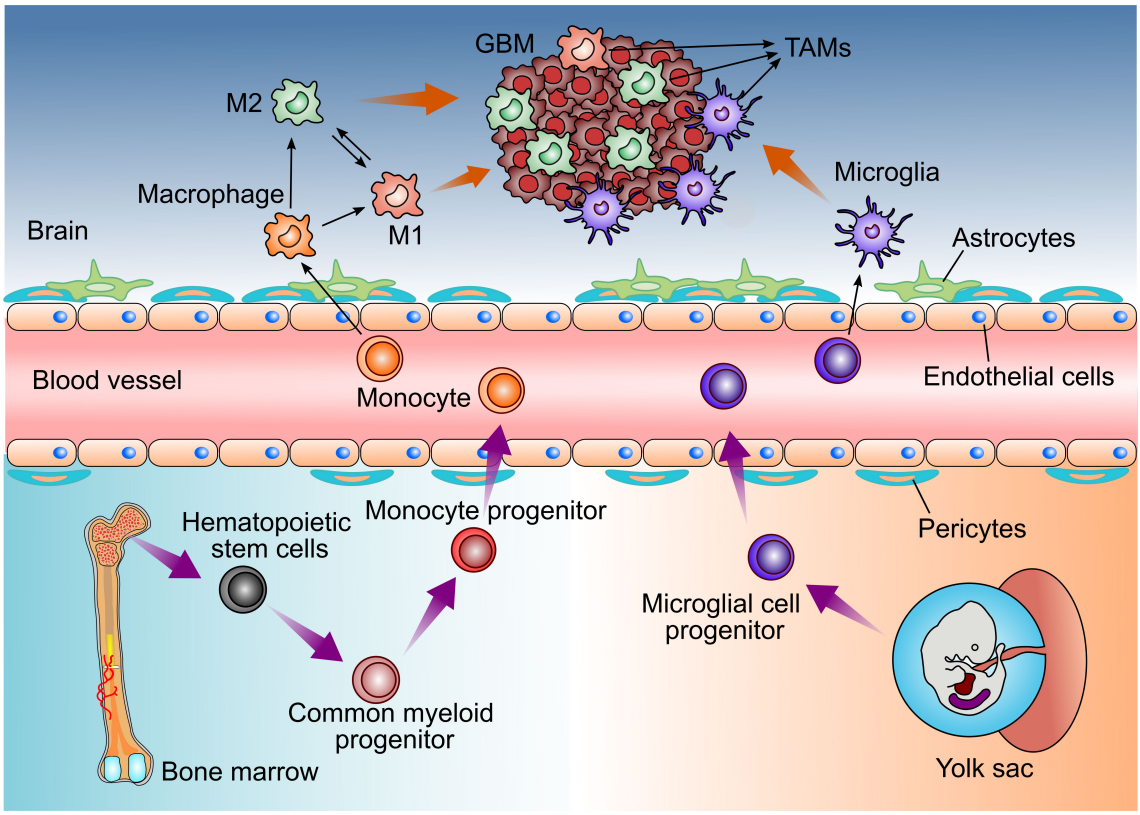

Figure 1.3 Tumor associated macrophages in glioblastoma (Wang et al., 2022)

1.2.2 Activation and Heterogeneity of TAMs

The heterogeneity of TAMs comes from their cellular origin, spatial localization, activation state, and transcriptional identity. Traditionally, they have been classified into two groups. M1 phenotype functions in pro-inflammation, characterized by classical activation of immune receptors TLR2/4 and produces pro-inflammatory cytokines like tumor necrosis factor. M2 phenotype functions in anti-inflammation and produces ARG1, IL-10, and IL-4 (Gordon, 2003). Additionally, it was considered that the GBM microenvironment exhibits an M2-like phenotype, predominantly to suppress immune reaction and support tumor progression. Current studies disclaim this hypothesis. In several GBM models, TAMs can co-express both M1 and M2 phenotype-related genes. Moreover, TAM heterogeneity also differs among GBM subtypes, which possess various molecular and immune landscapes. Mesenchymal subtype results in higher TAM infiltration into TME compared to the proneural subtype, with expression of different genes (Buonfiglioli & Hambardzumyan, 2021).

1.2.3 Functions of TAMs in GBM

Tumor-associated macrophages support tumor progression in several ways. Their key role is suppression of anti-tumor immunity that is mediated via expression of specific immune checkpoint molecules like Programmed Death-Ligand 1 (PD-L1) and secretion of different immunosuppressive cytokines like Interleukin-10. Moreover, they can express arginase-1 (ARG1), which decreases the L-arginine level and activates T cells. In addition to immunosuppression properties, they secrete hepatocyte growth factor (HGF), epidermal growth factor (EGF) and vascular endothelial growth factor (VEGF). These growth factors promote survival, cell proliferation and angiogenesis. Furthermore, they secrete matrix metalloproteinases that degrade ECM and promote migration of tumor cells into nearby brain tissues. Regrettably, they also act on therapeutic resistance via protecting cells from chemotherapy and radiotherapy by increasing survival signals and contributing to repair mechanisms. These factors make TAMs a critical target to figure out GBM biology and possible therapeutic approaches (Andersen et al., 2021; Sørensen et al., 2017).

1.2.4 TAM states invitro: M0/M1/M2

Three polarization states M0/M1/M2 are generally used in macrophage in vitro studies to estimate TAMs complexity in GBM. M0 macrophages, unpolarized cells, are derived from peripheral monocytes via treatment with macrophage colony-stimulating factor (M-CSF) or phorbol 12-myristate 13-acetate (PMA). After this treatment, M1 phenotype is obtained through exposure to lipopolysaccharide (LPS) and interferon-gamma (IFN-γ), while interleukin-4 (IL-4) or IL-13 stimulation can be used to obtain M2 phenotype (Baxter et al., 2020; Solomou et al., 2024).

Current advancement in profiling techniques suggests that TAMs in GBM are not closely associated with these classifications and they display hybrid or intermediate phenotypes. They can express M1 and M2 markers based on tumor signals (Solomou et al., 2024). Behind this complexity, this classification can be useful in in vitro studies to define macrophage activation. In this paper, the effects of these three macrophage populations on the behavior of glioma cells will be investigated.

1.2.5 Current Diagnosis and Challenges in GBM

Accurate diagnosis in GBM is very crucial to determine specific prognosis and treatment. Neuroimaging techniques are the primary methods for initial tumor detection. In imaging modalities, magnetic resonance imaging (MRI), the most preferred one, is used for visualization of tumor characteristics like uneven borders and lesions with their necrotic core. Additionally, positron emission tomography (PET) uses radiolabeled tracers to understand the metabolism of tumors and give insight into recurrence potential and treatment response. In parallel with imaging, histopathological analysis of biopsy samples is effectively used to confirm GBM diagnosis and to understand the genetic and epigenetic features of tumor cells. Molecular profiling of biopsy samples is significant for GBM classification. Despite current advancements in science and technology, accurate diagnosis and treatment of glioma is still challenging because of high tumor heterogeneity resulting in failure of standard tools, overlapped symptoms with neurological conditions (late response), risk of biopsy, and limited biomarkers. Microfluidic systems can be a new developing area to increase the diagnosis rate (Gough et al., 2025; Hosseini et al., 2023).

1.3 Comparison of Conventional Methods for Cell Separation

Heterogeneity of glioma cells and tumor microenvironment complicate glioma research in diagnosis and treatment. To characterize tumor behavior and its distinct subpopulations, the cell separation technique plays a critical role. There are two common conventional cell separation techniques: fluorescence-activated cell sorting (FACS) and magnetic-activated cell sorting (MACS). FACS can classify and analyze individual cells in a mixture of cells that are tagged with antibody-conjugated fluorescent dyes via optical measurements (Picot et al., 2012). MACS uses a combination of specific antibodies with magnetic beads that help to target markers on the cell surface. The tagged cells are sorted based on magnetic field gradient (Sun et al., 2015). These commercial techniques provide high-throughput screening; however, they have several limitations, including high costs for bulky machines and reagents (magnetic beads and antibodies), a large number of cells, and operational complexity (Nasiri et al., 2020; Sun et al., 2015). Additionally, centrifugation is a traditional method based on differences in cell density. It is used generally for blood samples to separate cells but it can result in immunophenotyping due to the high sensitivity of leukocytes to environmental changes (Gossett et al., 2010). Drawbacks of these techniques create a need for a practical and high-throughput technology with cost

efficiency.

1.4 Microfluidic Systems

Microfluidics systems are miniaturized devices that can function in cell separation by utilizing several properties of cells. Cell separation working mechanisms can differ, including inertial forces, filtration, hydrodynamic forces, and external forces. There are four methods using external forces. One of them is magnetophoretic cell separation based on the conjugation of targeted cells with nanoparticles by applying a magnetic field. This method is not proper for cells without intrinsic magnetic properties (Hejazian et al., 2014). Another one is the acoustophoretic cell separation technique that relies on the generation of an acoustic field via a sound reflector, ultrasonic transducer, or two sound sources being opposite. This system is label-free and shows high biocompatibility; however, its separation resolution is reduced because of the exhibition of the same sign's acoustic contrast factor by lots of cells (Fornell et al., 2018). In addition to these methods, optical forces can be used to separate cells via highly focused laser beams. Optical-based separation requires a bulky and expensive setup, and it is limited by label-free approaches (Atajanov et al., 2018; Nasiri et al., 2020). Another method that uses external forces, dielectrophoresis-based cell separation, where a non-uniform electrical field is applied to molecules that trigger movement of particles toward the electric field area (high or low). It is a label-free system, and cell viability is not significantly affected after the separation process (Henslee, 2020).

1.5 Dielectrophoresis

Dielectrophoresis (DEP) is an electrokinetic method that relies on a non-uniform electric field inducing polarization of cells based on their dielectric properties (membrane capacitance and internal conductivity). The response of cells can be toward higher or lower field strengths—defined as positive DEP (pDEP) or negative DEP (nDEP), respectively (Figure 1.4). The resulting force on these cells is called the DEP force, F_{DEP}. The equation for this force acting on spherical particles of radius

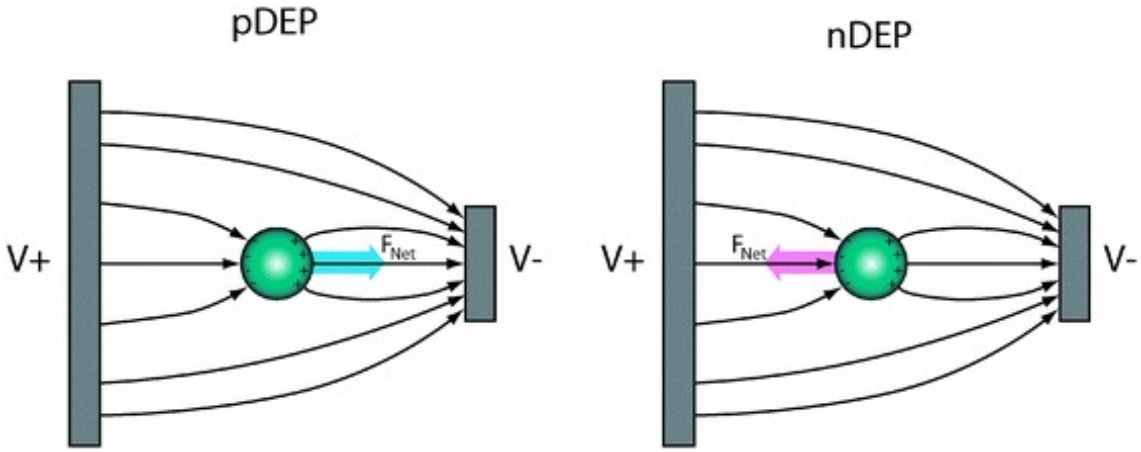

Figure 1.4 pDEP and nDEP responses. Particles move toward higher electrical fields in pDEP (left) while it is repelled in nDEP (Lenshof & Laurell, 2010).

R and permittivity ε_p in an electric field E within a medium of permittivity ε_m, is (Henslee, 2020; Maidin et al., 2021; Sarno et al., 2020):

$$F_{\mathrm{DEP}} = 2\pi\,\varepsilon_m\,R^3\,\mathrm{Re}\Big[K(\varepsilon_p,\omega)\Big]\,\nabla|\mathbf{E}|^2\,, \tag{1.1}$$

where $K(\varepsilon_p,\omega)$ is the Clausius–Mossotti factor,

$$K(\varepsilon_p,\omega) = \frac{\varepsilon_p - \varepsilon_m}{\varepsilon_p + 2\,\varepsilon_m}\,. \tag{1.2}$$

In a cell model, it is possible to see a membrane structure that covers the cytoplasm. These two components are critical for the CM factor, and change it. Therefore, the direction and magnitude of DEP force practised by cells are affected by the Clausius–Mossotti (CM) factor. pDEP and nDEP arise from CM factor differences, where cells are attracted or repelled by higher electrical strength, respectively (Hawkins et al., 2020). The switching point between these two forces is called the crossover frequency, where the CM factor is equal to 0. The crossover frequency of cells is their characteristic feature that helps to separate cells precisely (Giduthuri et al., 2020). Moreover, several research areas utilize DEP techniques for disease diagnosis (Adekanmbi & Srivastava, 2016), cancer detection (Chan et al., 2019), and cell separation (Sarno et al., 2020). These studies show that the DEP method is a useful choice for glioblastoma diagnosis and treatment. In this thesis, a DEP-based microfluidic chip is fabricated and tested for the selective manipulation of GBM cells.

1.6 Research Motivation and Aim

Glioblastoma multiforme is one of the most aggressive and lethal brain tumors, with its limited diagnosis and therapeutic options. Even with advances in technology and medicine, recurrence remains almost inescapable due to the infiltrative nature of glioblastoma cells, which communicate strongly with surrounding cells in the tumor microenvironment. Among the cellular components of the TME, macrophages are one of the dominant immune populations that are dynamically shaped by tumor-derived signals. They generally support tumor invasion and growth while creating immunosuppressive environments to hinder the effect of therapies (Louis et al., 2021; Andersen et al., 2021). Therefore, investigating interactions between tumor cells and macrophages is crucial for understanding glioblastoma progression and identifying new therapeutic targets.

The cellular heterogeneity in GBM is another critical barrier. Conventional methods generally fail to distinguish and separate glioma cells from surrounding cells, which limits analysis of tumor intrinsic properties. Microfluidic systems combined with the dielectrophoresis method is an innovative and label-free technique to separate glioma cells from their surroundings and increase the knowledge on their heterogeneity. This technique preserves cell viability which allows further functional studies (Nasiri et al., 2020; Henslee, 2020). This approach is promising to dive into tumor heterogeneity and to develop precise diagnostic and therapeutic aspects.

The aim of this study is twofold: to investigate the influence of monocyte-derived macrophages on GBM cell growth and migration, and to fabricate a microfluidic DEP-based chip for glioma cell separation from its surrounding microenvironment. This thesis aims to contribute to the literature by providing a deeper understanding of tumor-immune interactions and advancing cell separation techniques through a combination of biological and engineering perspectives.

2. MATERIALS & METHOD

2.1 Cell Culture

2.1.1 U-87 Cell Culture

The U87-MG (HTB-14™) human glioma cell line (obtained from ATCC®) was cultured in Dulbecco's Modified Eagle Medium (DMEM, Gibco) enriched with 10% heat-inactivated Fetal Bovine Serum (FBS, Gibco) and 1% Penicillin/Streptomycin. Culturing conditions of cells were supported by the NUVE cell culture incubator with 5% CO_2 at 37°C. In addition to standard culture conditions, U-87 cells were also cultured in a mix conditioned medium (CM) obtained from culturing of monocyte-derived macrophages (MDM) in Roswell Park Memorial Institute Medium 1640 (RPMI 1640, Gibco) medium for 48 hours. The obtained media is mixed with complete DMEM media in a 1:1 ratio.

2.1.2 THP-1 Cell Culture

THP-1 (TIB-202 ™) human monocytic cell line (obtained from ATCC®) was cultured in RPMI 1640 supplemented with 10% FBS and 1% Penicillin/Streptomycin in incubator with 5% CO_2 at 37°C.

2.2 Monocyte Derived Macrophage Differentiation

THP-1 cells were used to differentiate monocytes to macrophages. 2.5 x 10^5cells/ml were seeded into each well of 6-well plate in 2 ml complete RPMI 1640 media. Phorbol 12-myristate 13-acetate (PMA, Pan Biotech, Germany) was diluted with dimethyl sulfoxide (DMSO, Pan Biotech, Germany) to obtain 100 µg/ml stock solution. 1 µl of this solution was added into each well to achieve a final concentration of 50 ng/ml and mixed carefully in the dark. Cells were incubated for 48 hours at 37°C incubator. PMA is light-sensitive; therefore, cells are protected from light. After 48 hours of incubation, fresh medium was added into each well and incubated for 24 hours to allow cells to rest. M0-type macrophages were ready for use. After resting period, Lipopolysaccharide (LPS, Sigma-Aldrich) was added into wells to a final concentration of 100 ng/ml and recombinant human Interferon gamma (rhIFN-γ) of 20 ng/ml to stimulate M1 macrophages, while recombinant human Interleukin 4 (rhIL-4) and recombinant human Interleukin 13 (rhIL-13) were added at 20 ng/ml final concentration for stimulation of M2 macrophages. These cells were incubated for 24 hours with stimulation factors, and media were changed with fresh complete media after incubation (Figure 2.1a).

2.3 Conditioned Media Preparation

After completion of the differentiation process, cells were incubated for 48 hours with fresh media. After this period, the media was collected and centrifuged at 3000 rpm for 5 minutes. This media was filtered via a syringe connected with a 0.2 µm filter.

2.4 Monocyte differentiation in Tumor Conditioned Media and Flow

Cytometry

300.000 U-87 cells were seeded into a 25 ml flask and incubated for 48 hours. After incubation, the media were collected and centrifuged at 1800 rpm for 5 minutes. Filtration was applied to remove any residual part via 0.2 micrometer filter. THP-1 cells were seeded into three different media: RPMI 1640 (control), 50% RPMI 1640 + 50% DMEM (media control) and 50% RPMI 1640 + 50% conditioned media derived from U-87 incubation. 400.000 cells were seeded into each well of a 12-well plate in 1 ml media. The incubation period was 7 days. Cells were prepared for flow cytometry analysis to see changes in cluster of differentiation markers CD11b and CD14.

THP-1 cells were centrifuged and resuspended in Phosphate Buffered Saline (PBS). Centrifugation was repeated to resuspend cells with washing buffer (19 ml PBS + 1 ml FBS). Primary antibodies; CD14 (ab181470) and CD11b (ab52478) were added and incubated for 30 minutes on ice in the dark. After incubation, cells were washed with a washing buffer three times, and a second incubation was started with the addition of a secondary antibody (goat anti-mouse Alexa Fluor 488 (ab150113)) which was washed away with washing buffer after 30 minutes of incubation on ice. Finally, cells were resuspended in 500 µl washing buffer. CD14 and CD11b levels were analyzed in flow cytometry (Beckman Coulter CytoFLEX).

2.5 Growth Curve

To understand the effect of macrophages on glioma cell growth, 3.000 U-87 cells were seeded into each well of 96-well plate in 200 µl. There were 6 different groups: U-87 in DMEM media (control), U-87 in 50% DMEM & 50% M0 conditioned media, U-87 in 50% DMEM & 50% M1 conditioned media, U-87 in 50% DMEM & 50% M2 conditioned media, and U-87 in 50% DMEM & 50% RPMI 1640 (media control). Wells were arranged like every experimental group has three wells for each analysis day. The Cell Counting Kit-8 (CCK-8, (Elabscience Enhanced Cell Counting Kit 8)) method was applied to find the viability of cells. Firstly, the media was discarded, and a CCK-8 solution (10 µl CCK-8 + 100 µl DMEM) was added to each well. After 3 hours of incubation, absorbance values were taken at 450 nm from a microplate reader (Tecan Infinite M200 Pro). The growth was checked in the 1st, 3rd, 4th, 5th and 7th days (Figure 2.1b).

2.6 Wound Healing

U-87 cells were seeded into a 6-well plate. When they reached 80-90% cell confluency, vertical stretches were opened via 200 µl pipette tip. Complete DMEM media was added to one well to observe normal cell migration, while the other wells contained MDM-conditioned media in a 1:1 ratio. To be able to compare results, cells were stained with Hoechst 33258 and Propidium iodide (PI) after 48 hours incubation. Confocal microscopy (Zeiss LSM 710) images of samples were analyzed via ZEISS ZEN 3.12 software. To be able to present the direct wound percentage, U-87 cells were seeded into a 6-well plate and after reaching confluency vertical stretches open with 1000 µl pipette tip. Same conditions were applied without staining and images were taken in an inverted light microscope at 4x objective after 24 and 48 hours incubation (Figure 2.1c).

2.7 Co-Culture

10.000 U-87 cells were cultured with 20.000 M0 macrophages in 1:1 DMEM and M0 conditioned media. Cells were incubated for 6 days and after 72 hours fresh combined media was added into the system. Microscope images were taken for each day at 10x objective.

2.8 Design of Microfluidic System

SolidWorks programme was used for designing microfluidic chips. The design includes electrodes with a diameter of 200 µm/height of 100 µm placed at 200 µm intervals and a channel with a depth of 100 µm. The distance between two electrodes in two layers was arranged to 400 µm, center to center. The size of the microfluidic chip is 77 mm x 27 mm, and the area occupied by the electrodes is 6 mm x 2.3 mm. The cylinders in design represent the electrodes, while the blue and black lines indicate the positive and negative electrode connections, respectively

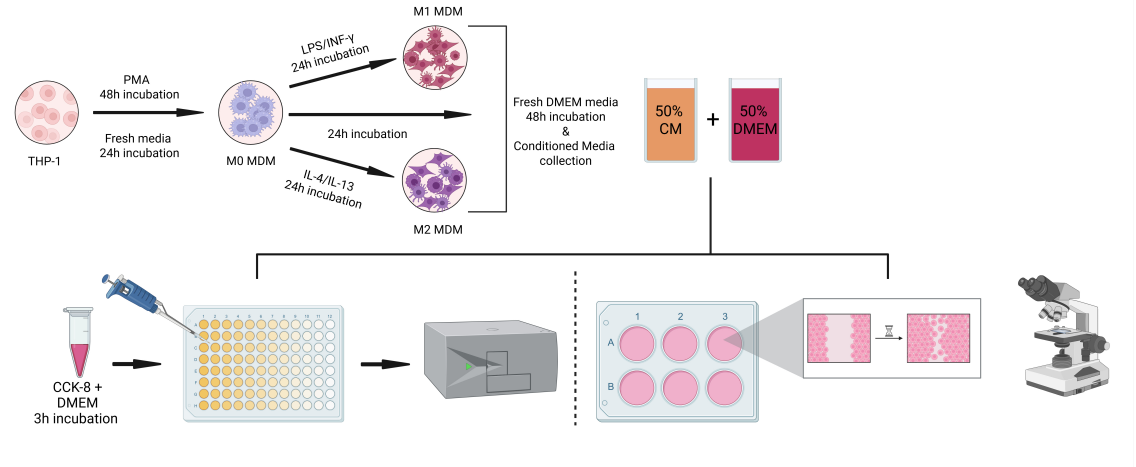

Figure 2.1 Experimental set-up of monocyte-derived macrophages. THP-1 differentiation to macrophages (a); use of its conditioned media for cell growth analysis (b) and wound closure (c) (created with BioRender).

(Figure 3.8a). In cell separation, the shear rate of the buffer solution is a critical factor to consider, especially in designs aimed at capturing a specific cell type (Sun, 2016). The biophysical properties of cells exposed to high shear rates may change (Jiang et al., 2019). Therefore, the electrode geometry was designed as symmetrical horizontal cylinders to both reduce the shear rate affecting the cells and enhance their retention on the electrodes through positive DEP (pDEP) (Zhang et al., 2019). The design was separately created for the production of two different masks.

2.9 Simulation

The electric field distribution and flow velocity within the microfluidic chip were simulated using the Comsol Multiphysics software (version 6.1). In this simulation, the Electric Currents and Creeping Flow modules were used to determine the electric field distribution. The flow profile within the microfluidic device was calculated based on the Navier–Stokes and Fick's laws. An electric potential ranging from –5 Vpp to 5 Vpp, with frequencies between 10 kHz and 10 MHz, was applied to the electrodes to analyze the electric field distribution both in static conditions and in the presence of flowing cells within the DEP buffer solution.

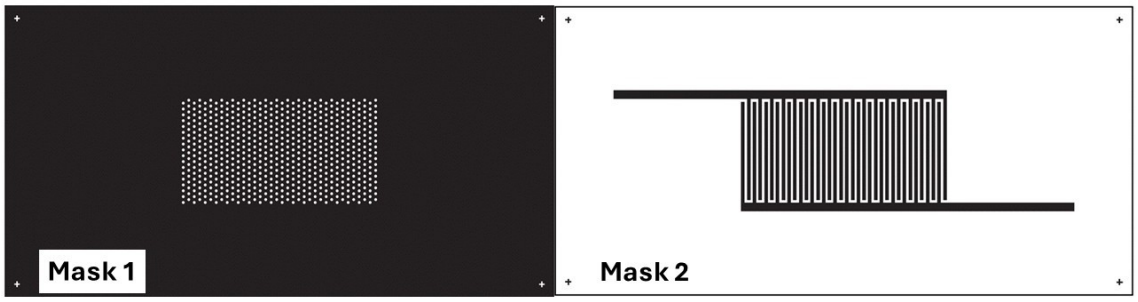

Figure 2.2 Designated masks for chip fabrication. Mask 1 and Mask 2, respectively.

2.10 Fabrication of Microfluidic Device

The optimal microfluidic device design determined through simulation was fabricated using well-established soft lithography and electron-beam evaporation techniques (Figure 2.4). To fabricate the microfluidic device, two masks were designed (Figure 2.2). Mask 1 was designed as the first photolithographic mask used to define the geometry of micro-pillars via SU-8 negative photoresist. It was designed as a dark-field mask in which only the electrodes are white, allowing SU-8 electrodes to be formed under UV light. Mask 2 was designed to pattern a network of electrodes interconnecting SU-8 micro-pillars. These interconnections are important for the spatially uniform electric field for the effectiveness of dielectrophoretic manipulation.

First, SU-8 3050 negative photoresist was spin-coated onto a glass wafer. To be able to obtain an 80-85 µm SU-8 layer, a specific spin-coating recipe was applied (Table 2.1). SU-8 is an epoxy-based material that forms a chemically and mechanically stable structure after UV exposure. In negative photoresist, white parts exposed to UV become crosslinked. On the other hand, black parts become soluble and wash away. After coating, a soft baking process was carried out to improve the adhesion of the photoresist to the substrate, stabilize the resist layer, and ensure a homogeneous, solvent-free coating. This process began with an initial 5-minute bake at 65°C to promote the evaporation of residual solvents. After baking, the SU-8-coated glass wafer was exposed to UV light through an electrode mask at an intensity of 13.4 mW/cm² for 20 seconds, resulting in the formation of pillars. Post-exposure baking was applied to reinforce the cross-linking of the exposed SU-8 regions (Table 2.1). Then, the sample was placed into a flask containing SU-8 developer for nearly 8 minutes to remove unexposed material. Formed micro-pillars were evaluated under microscopy (Figure 2.3a).

Table 2.1 Spin-coating and baking parameters for SU-8 3050.

SU-8 3050 Coating			
Step	Duration (s)	Spin speed (RPM)	Acceleration (RPM/s)
1	10	500	200
2	45	2000	200
3	5	0	200

Pre-Exposure Baking		
Step	Temperature (°C)	Duration (min)
1	65	5
2	95	15

Post-Exposure Baking		
Step	Temperature (°C)	Duration (min)
1	65	2
2	95	10

To create electrical functionality, a metallic aluminum layer deposition was done via electron beam evaporator system. 1 µm thickness of aluminum on our glass wafer was obtained (Figure 2.3b). The conductivity, affordability, and compatibility of aluminum with fabrication systems make it a suitable choice for our microchip fabrication.

Table 2.2 Parameters for coverage of electrodes with AZ 4620 photoresist.

AZ 4620 Coating			
Step	Duration (s)	Spin speed (RPM)	Acceleration (RPM/s)
1	10	500	200
2	45	2000	200
3	5	0	200

After the formation of the aluminum layer, positive AZ4620 photoresist was spin coated onto glass wafer with a uniform 10 µm thickness (Table 2.2). In the second lithography part, Mask 2 was used to form a micro-pillar array. The mask was aligned with the phoresist and aluminum-coated glass wafer. UV exposure was applied for 40 seconds. Soft baking was performed at 110°C for 4 minutes to evaporate solvents and stabilize the resist layer. Then, wafer was immersed in AZ developer

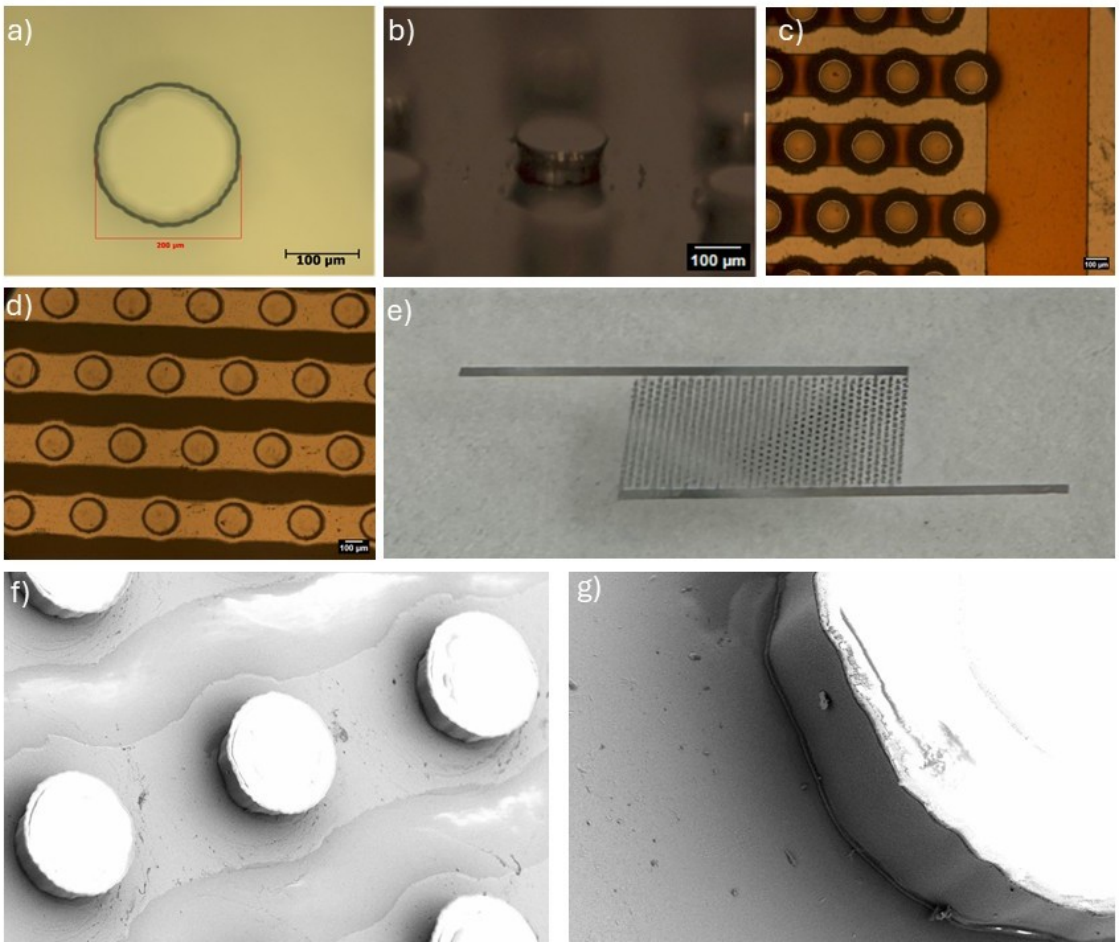

Figure 2.3 Representation of results after fabrication steps. SU-8 pillar (a), aluminum-coated SU-8 pillar (b), after AZ 4620 development (c), final microscopic image (d), final version with eyes (e), and SEM images of fabricated chip (f, g).

solution for dissolution of the exposed positive photoresist for 10 minutes. As a final step, chemical etching was applied and only the regions protected by AZ4620 remained covered (Figure 2.3c). This ensured our design with defined and conductive electrode connections. Figure 2.3d shows chip image under light microscope, and Figure 2.3e shows how it is seen with eyes. Furthermore, scanning electron microscopy (SEM) imaging was conducted as the final step to evaluate the structural integrity of the fabricated microfluidic chip (Figure 2.3f,g). Finally, cables were pasted on electrode lines to connect our chip system to the empedens device and oscilloscope.

2.11 DEP Buffer Preparation

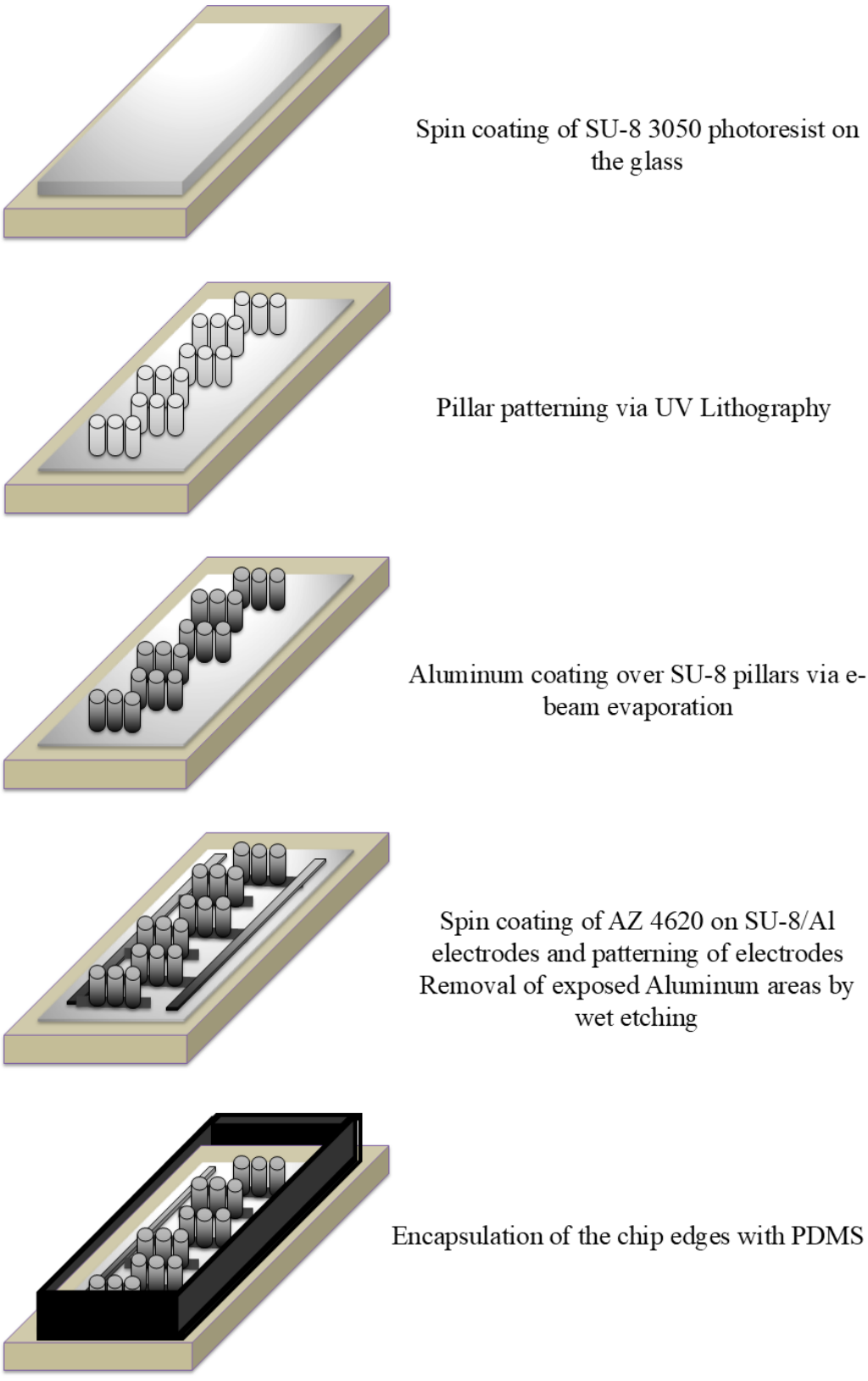

Figure 2.4 Fabrication steps of microfluidic chip.

To obtain a low conductive DEP buffer, 8.6% sucrose (BioFroxx), 0.3% glucose (Sigma Aldrich), and 0.1% Bovine Serum Albumin (BSA, PAN Biotech) were solved in deionized water. To decrease unwanted residues in our buffer, mixed solution was filtered through a 0.22 µm filter. Finally, the conductivity level was measured as 20 µS/cm via the conductivity meter (CORNING, 311 Conductivity).

2.12 Viability in DEP Buffer

U-87 cells were detached from the cell culture flask and centrifuged at 1800 rpm for 5 minutes. The media was removed and the remaining pellet was dissolved in the DEP buffer. This step is repeated one more time to avoid effects of previous DMEM media which have different and higher conductivity. In the final washing, cells were dissolved in a 1 ml DEP buffer in eppendorf tubes and incubated in 37°C for 30 minutes. Before and after incubation viable cells were stained with trypan blue and counted with hemacytometer. The difference between each group was noted and the experiment repeated for three times.

2.13 Impedance Measurement and Finding Cross-over Frequency

The chip system was connected with two wires to create a simple two-terminal configuration as shown in Figure 2.5a. Set-up was arranged to 100 mV AC and 100 Hz/1MHz frequency range. 500 µl of U-87 cell/DEP suspension was placed onto our chip having a PDMS well structure.

After finding specific frequencies, the chip system (Figure 2.5b) was connected to an oscilloscope and system placed onto a light microscope stage. 1 Vpp and 2 Vpp were applied. 50 kHz was chosen as the start point and 1.3 MHz as stop point. At each frequency, nearly 30 seconds were waited and TIFF images were captured using the light microscope and analyzed with ImageJ software.

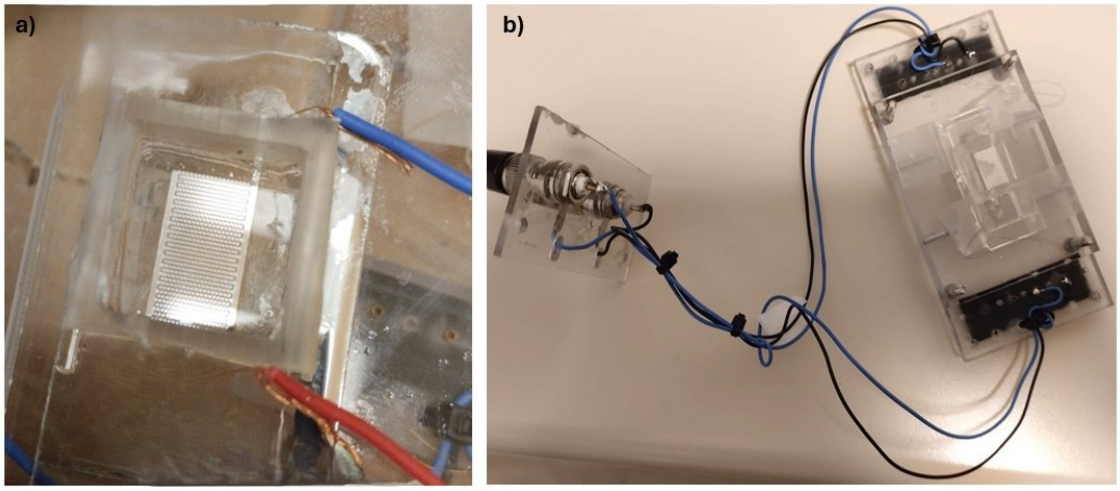

Figure 2.5 Two systems to connect our microfluidic device to machines. Wiring of chip for impedance measurement (a) and oscilloscope (b).

3. RESULT & DISCUSSION

3.1 Differentiation of Monocytes into Macrophages

To assess the differentiation of monocytes to macrophages, physiological changes seen in MDM were observed. 2.5×10^5 cells/mL of THP-1 cells were triggered to differentiate in the presence of 50 ng/ml PMA for 48 hours. Gopinath et al. (2020) showed that this concentration and incubation time is preferable because of the very low number of non-adherent cells after treatment. Liu et al. (2023) also found that the proliferation activity of THP-1 cells is negatively affected when PMA concentration is higher than 200 ng/ml. The lower concentrations showed similar proliferation capacity compared to normal growth conditions. In our experimental part, we followed suggested values. For polarization of M0 macrophages into M1 and M2, 100ng/ml LPS + 20ng/ml INF-γ and 20ng/ml IL-4 and IL-13 were used, respectively.

THP-1 cells are round shape suspension cells. After PMA treatment, they started to attach onto the surface which is characteristic of macrophages (Figure 3.1b). After PMA treatment, macrophages stay in the resting phase like an adherent circle shape. It is possible to see shape differences on cells after M1/M2 stimulation, and incubation of M0 macrophages for a long time also trigger several morphological changes. In Figure 3.1c, there are spindle-like, satellite, and fried egg (Mahmoudian et al., 2025) macrophages. In particular, spindle-like shapes are linked with the pro-inflammatory effect of M1 macrophages (Ribeiro et al., 2021). From our images, it can be claimed that the number of spindle-like cells is high in LPS/INF-γ treated M0 macrophages.

Morphological changes are the first part of a qualitative indicator of macrophage differentiation. There should be several quantitative data to distinguish polarization

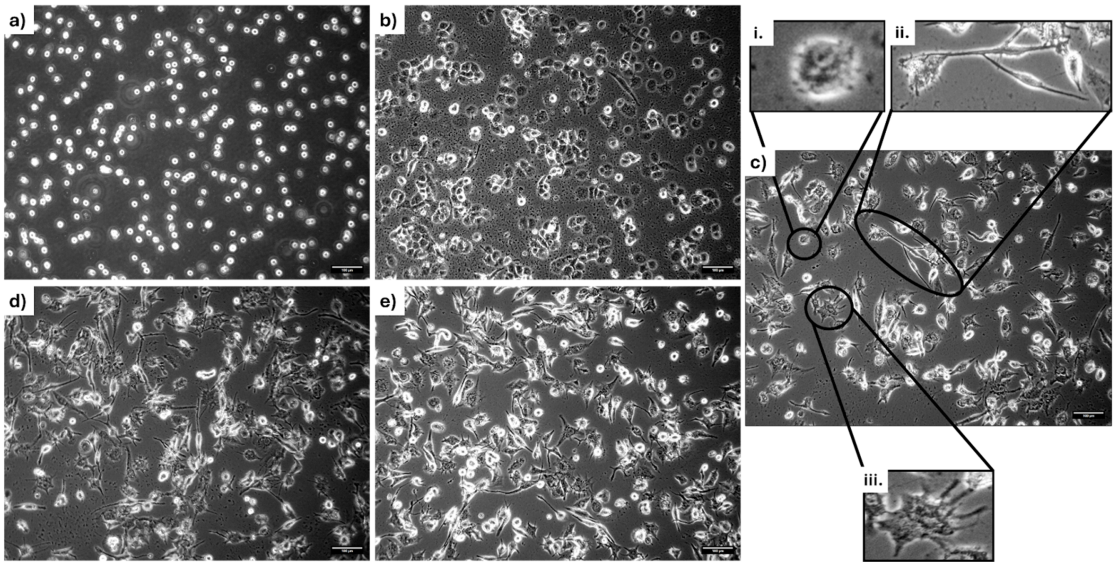

Figure 3.1 Morphology of cells in differentiation and polarization processes. THP-1 cells (a), THP-1 cells after 48 hours PMA incubation (b), M0 macrophages after 3 days of differentiation (c), (i. fried egg, ii. spindle-like, and iii. satellite morphologies), M1 polarization after 24 hours of LPS/INF-γ stimulation (d), and M2 polarization after 24 hours of IL-4/IL-13 stimulation (e). All images were captured at 10x. i. 70 μm, ii. 273 μm and iii. 123 μm are zoomed in the form of 10x objective images.

states. In our M1/M2 macrophages both show three different morphologies that support their heterogeneity and their high plasticity even under in vitro conditions. Additionally, the heterogeneous nature and plasticity of MDMs is a critical research area to understand their specific role in glioblastoma tumor microenvironment where their interactions affect tumor progression, immune evasion and resistance to therapeutic approaches.

3.2 THP-1 Cells Tend to Differentiate in Glioblastoma Conditioned Media

To understand the effect of GBM-derived soluble factors on monocytes to trigger macrophage differentiation, THP-1 cells were grown in U-87 conditioned media for 7 days. The expression of CD14 and CD11b surface markers, well-known surface markers related with macrophage activation and differentiation, were analyzed via flow cytometry. A standard gating strategy was applied to exclude dead cells, debris and doublet cells which ensures that only single cells are analyzed for surface marker

expression (Figure 3.2a). Gating was started with viable cells and continued with single cells and fluorescence-positive cells. This system was applied to the unstained THP-1 cells to increase accuracy.

As media controls, THP-1 cells were grown in RPMI 1460 alone and 1:1 RPMI/DMEM. DMEM media was used because it is normal growth media for U-87 cells. Additionally, conditioned media was mixed with fresh RPMI media to support cells with essential ingredients that are lacking in conditioned media. In Figure 3.2a, the expression levels of $CD11b^+$ and $CD14^+$ in both media controls were similar. These represent that DMEM medium has no effect on THP-1 cells differentiation. Furthermore, even percentages of these two controls are similar; they show expression. This can be because of an increased number of cells in long term incubation and nutrient depletion that trigger spontaneous differentiation. Lomovskaya et al. (2022) suggest that high cellular density (inhibition of cell growth and cell death activation) of THP-1 cells in in-vitro culture conditions results in a macrophage-like phenotype that shows cell adhesion to the surface.

In U-87 conditioned media for a week showed increased expression in $CD11b^+$ (24.2%) and $CD14^+$ (25.5%) populations compare to control groups. This result is correlated with the current literature that CD11b and CD14 expression level increases nearly 1.5 fold with the activation and polarization of THP-1 cells (Chowdhury et al., 2024). This shows that glioma cell secreted cytokines enhance reprogramming of immune cells and promote accumulation of tumor-associated macrophage population in its microenvironment.

To identify which specific soluble factors function in the differentiation process, there should be further experiments such as mass spectrometry-based proteomics, multiplex cytokine profiling and enzyme-linked immunosorbent assay (ELISA). Additionally, parameters such as initial seeding density and incubation time may influence the concentration of secreted soluble factors. Our initial results can be compared with future experiments containing several cell density levels and incubation times to understand the temporal and dose-dependent nature of GBM-induced immune modulation.

3.3 Cell Proliferation of Glioma Cells

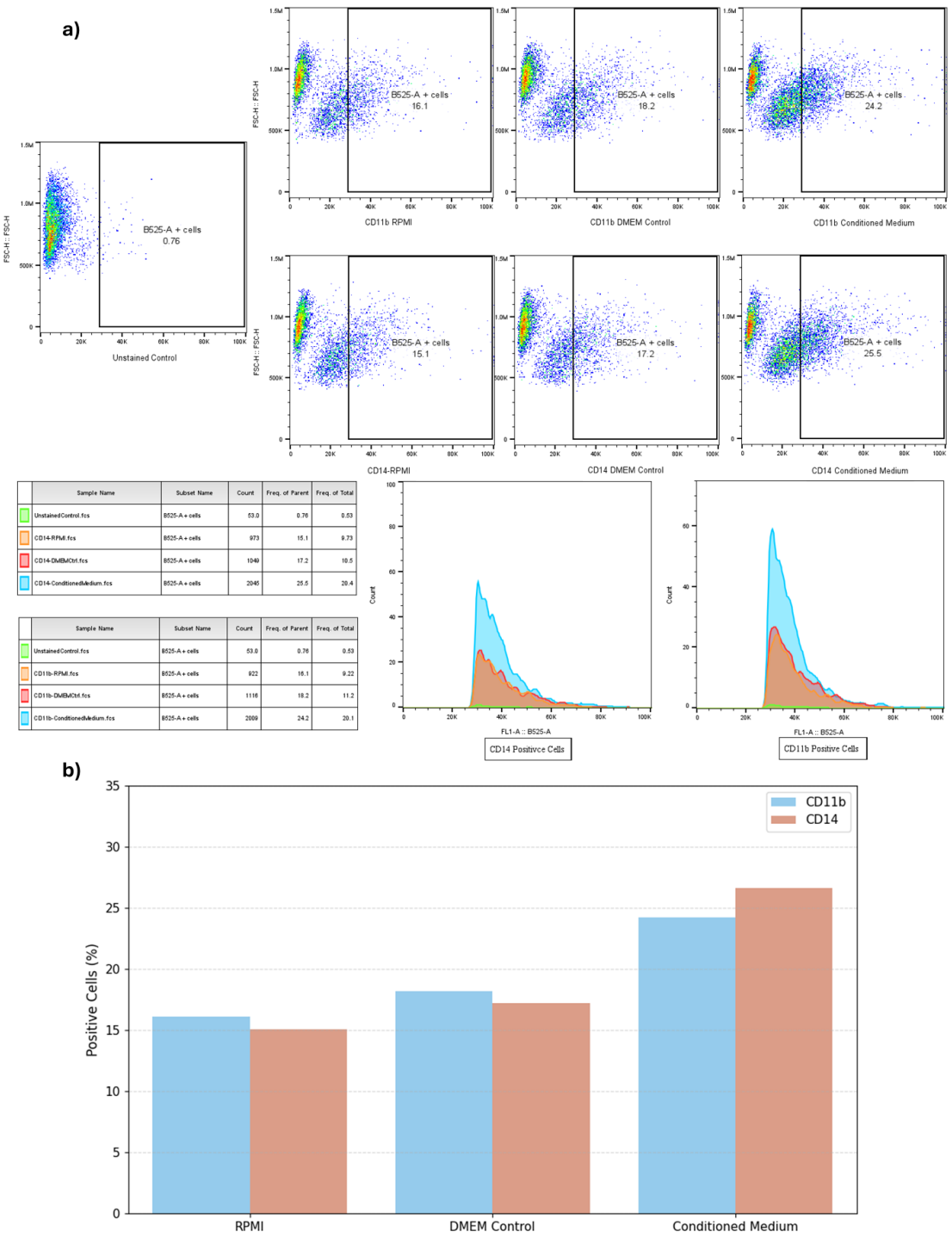

Figure 3.2 Tendency of monocytes to differentiate under glioma conditions. The flow cytometer results of $CD11b^{+}$ ve $CD14^{+}$ expression; gating hierarchy is viable cells $\rightarrow$ single cells $\rightarrow$ positive cells (a), and bar graph of $CD11b^{+}$ ve $CD14^{+}$ cells in control and tumor CM conditions (b).

To investigate the effect of different MDMs on glioma cell proliferation, CCK-8 reagent was applied to cells that grew in 1:1 DMEM/conditioned media at multiple time points: days 1, 3, 4, 5, and 7. The CCK-8 reagent is used to measure activity of intracellular NAD(P)H-dependent dehydrogenases, reducing water-soluble tetrazolium salt to a colored formazan product. This enzymatic activity correlates with the metabolic activity of viable cells, and it is quantified by measuring absorbance at 450 nm (Fan et al., 2024). Figure 3.3 represents two independent experiment results and their mean values with error bars.

In all conditions, glioma cells showed a rapid increase in the absorbance level which indicates active proliferation until day 3. It is possible to see divergent patterns from day 4 and onward depending on macrophage conditioned medium. In the first experiment (Figure 3.3a), DMEM and RPMI media showed a similar trend as expected positive controls. Interestingly, U-87 cells grown in M1 macrophages represent higher metabolic activity compared to those in M0 and M2 media, particularly after the fourth day. The absorbance level of cells in M0 media showed slight decreases at day 4, and followed by a rapid increase. Furthermore, M2 CM resulted in a clear decrease that continues with an important increase in cell viability in both experiments. This claims that soluble factors secreted by M2 type macrophages initially suppress proliferation however, it results in subsequent recovery with an increase in cell viability. Additionally, there is no big difference, but also M0 conditioned media shows similar trend to M2 CM. It shows an intermediate effect on cell growth between M1 and M2 conditioned media. These results underline the dynamic influence of macrophage secreted factors on glioma cell proliferation. M1 macrophages enhance the proliferation while M2 macrophages suppress and then support the cell growth.

These findings suggest that polarization states affect the behaviour of glioma cells differently, showing their functional plasticity. Compared to classical knowledge in literature, M1 and M2 in vitro phases suggest that M1 should inhibit cell growth while M2 should enhance glioma cell proliferation (Wang et al., 2024). Our results showed that the transient suppressive effect of M2 macrophages and increased proliferation under M1 macrophages. However, if we compare them with DMEM control, M1 CM proliferation level is not higher than the positive control. There is no additional increase in proliferation.

Șovrea et al. (2022) showed that expression of high tumor necrosis factor alpha (TNF-α) secreted by M1 macrophages was found in glioma patients and they correlated it with glioma progression and proliferation. Several cytokines function in different pathways but their activation can activate other pathways. Because of this

complexity as well, working on the interaction between glioma and macrophages is challenging. Another reason can be that soluble factors coming from conditioned media can be unstable or degraded by enzymes. Therefore, the 3rd or 4th day can be considered the optimal time for this experimental procedure. In the M1 case, there is also another possibility is that even with the same procedure and same cell density applied for differentiation, cytokine levels are correlated with differentiation efficiency and number of differentiated cells. Additionally, two points are coming from M0 (day 7) and DMEM (day 5) data in Figure 3.3b. Compared to the first experiment, these data points show an outlier effect. These unspecific decreases can be correlated with an initial lower cell quantity in these wells. There should be a supportive cell proliferation assay to prove the reliability of CCK-8 based proliferation.

3.4 Migration Capability of Glioma Cells Under MDM Conditioned Media

To determine the effect of monocyte derived macrophages on GBM cell migration, U-87 cells were seeded and wound area was created after they reached confluency. In Figure 3.4a, there is a panel of confocal images taken before and after incubation time points with Hoechst 33258 and PI staning where nucleus staning and death cell staning applied, respectively. Numerically, the wound area represented with pink irregular shape and intensity of stains (Figure 3.4b) give some information about migration capability. GBM grown in DMEM condition media shows the highest Hoechst intensity meaning high cell density in a specific area. As expected DMEM control shows robust cell proliferation and minimal cell death. M0 and M2 macrophages represent similar intensity levels while M1 CM shows higher effect on cell migration. Additionally, the highest cell death (PI/Hoechst ratio) is seen in M2 CM which is corresponding with the previous cell proliferation graph. It is higher than DMEM and M0 CM controls but their difference is not huge; they show a parallel effect on cell death in wound area. Based on M1 CM PI/Hoechst ratio, soluble factors of M1 macrophages resulted in the least cell death, which also corresponds with previous findings.

To quantify wound area, the same conditions were applied as in the previous one. The stretch was opened via a 1000 µl pipette tip differently. Images were analyzed through ImageJ software. Figure 3.5 represents the microscope images with the cor-

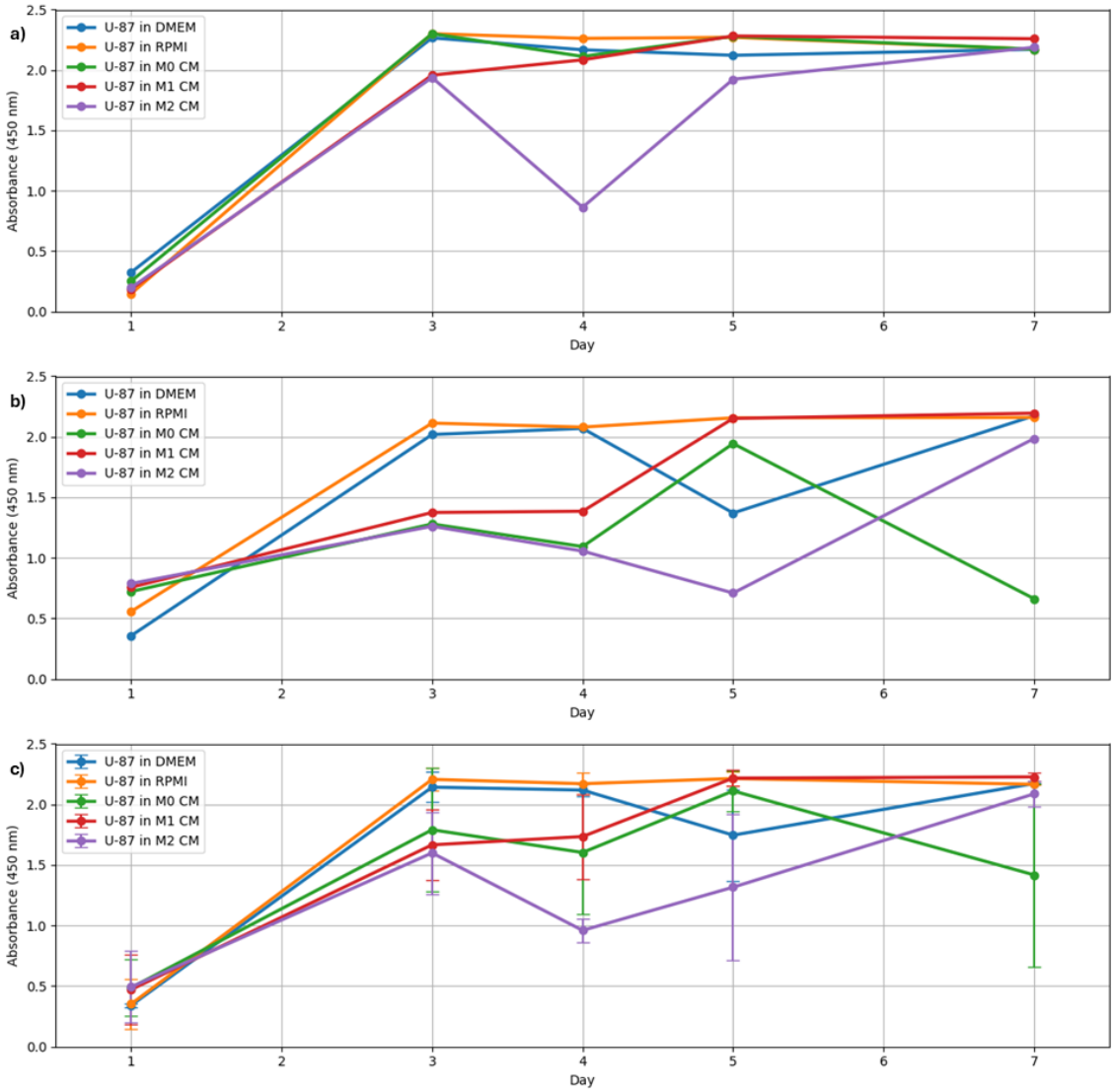

Figure 3.3 Growth curve of U-87 cells cultured in different media conditions based on absorbance (450 nm) values measured via CCK-8 assay. The first experiment (a), the second experiment (b), and the mean of two experiments with error bars (c).

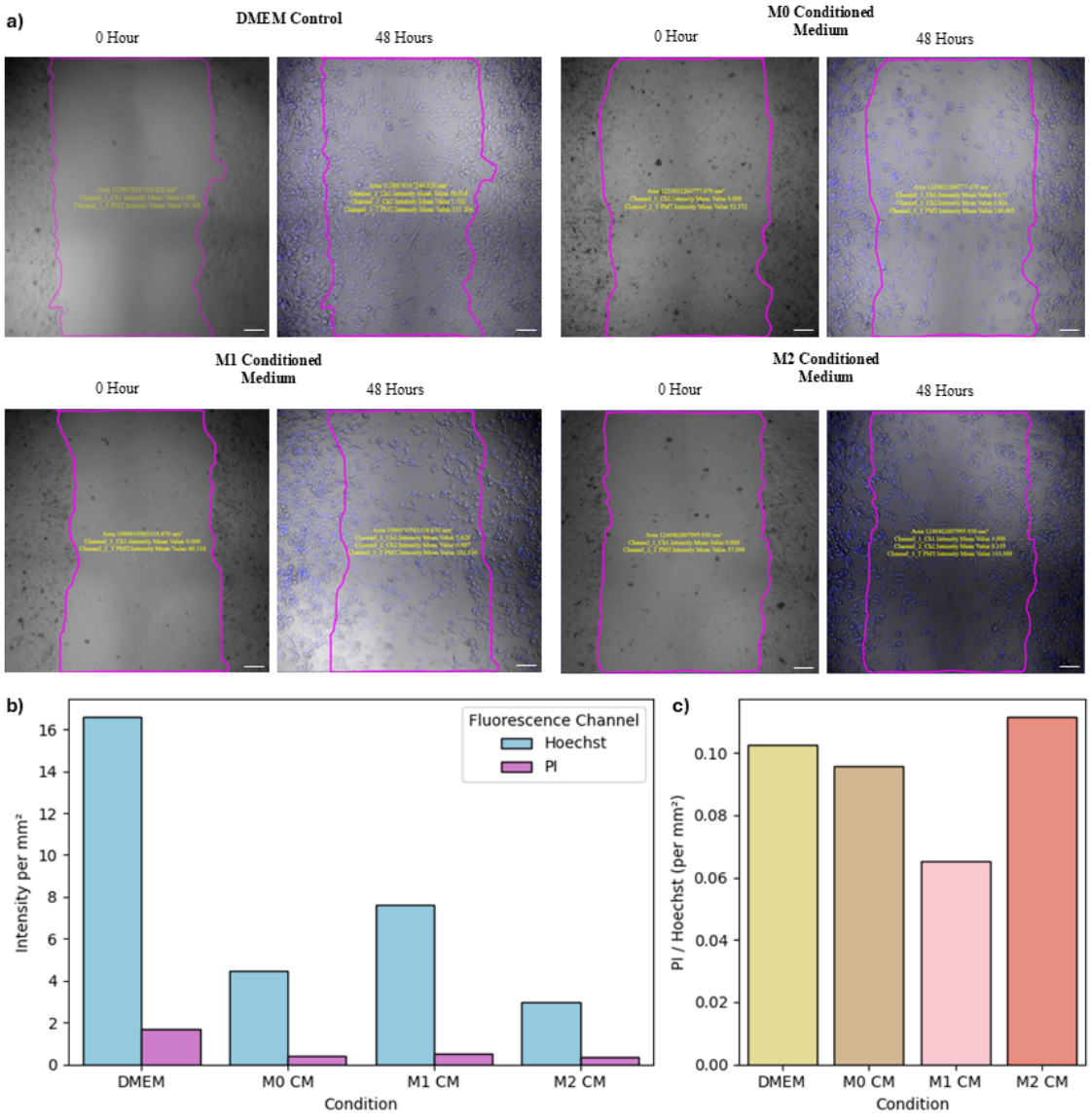

Figure 3.4 Wound closure of U-87 cells for 48 hours in different conditioned media. Confocal images of U-87 cells in DMEM, M0 conditioned media, M1 conditioned media, and M2 conditioned media, after wound creation (left) and after 48 hours of incubation (right) showed in a. Hoechst 33258 and PI dyes were applied after 48 hours of incubation. The pink irregular shape represents the wound area created at 0H and this pink line is applied to the 48H images. Yellow labels represent area in nm^2 and intensities of stains. Intensity comparison of Hoechst 33258 (blue) and Propidium iodide (pink) (b), where cell death analysis in the wound area was performed. PI dye shows dead cells while Hoechst 33258 dyes the nucleus. The scale bar for each image is 100 µm.

responding wound area percentage to total image. Each condition shows a decrease in wound area compared to their initial wound area. Additionally, M1 CM shows its resistance to migration compared to other groups when wound closure percentage is checked (Figure 3.6). This is correlated with literature that M1 macrophages work as anti-inflammatory, decreasing cell migration. M0 and M2 macrophages represent positive control behaviour supporting cell migration.

When these two migration results are compared, we can see that results are not correlated within CM groups. Normally, M2 macrophages should support migration while M1 macrophages prevent cells from migration. M2 macrophages are able to secrete transforming growth factor beta (TGF-β) and CCL18 which are responsible for epithelial mesenchymal transition (EMT) and migration (Chen et al., 2019). Migrating cells or cells transitioning into a migratory phenotype have exhibited reduced adherence. In the confocal imaging based experiment, cells were stained and washed several times which resulted in the loss of weak adherent cells during sample preparation. This could explain the lower Hoechst intensity observed in the M0 and M2 CM groups, despite their higher migration potential. Future experiments may focus on identifying and quantifying specific soluble factors secreted from macrophages involved in the regulation of glioma cell migration.

3.5 M0 Macrophages and Conditioned Media Trigger Senescence

To demonstrate the morphological effect of monocyte derived macrophages on GBM cells, U-87 cells were co-cultured with M0 macrophages. There are several morphological differences in a time dependent manner. After 48 hours of incubation, cells started to exhibit subtle elongation and cytoplasmic expansion compared to normal cell morphology seen in Figure 3.7f. This shift started to become evident where the majority of cells showed flattened and spindlelike structure with extension in cytoplasm at 72 hours (Figure 3.7c). After 120 hours, some cells showed distinctly enlarged cytoplasmic areas and flattened morphology while reducing clustering. It can be claimed that these features are related with cytoskeletal remodeling and may suggest alteration in adhesion dynamics and enhanced migration capability. Additionally, these enlarged cytoplasm and flattening can be related to the early senescence phenotype (Yang et al., 2017; Beck et al., 2020). This is not a quantitative result; it can be assumed on prolonged incubation of U-87 cells in conditioned media, which also lack the required fresh media gradients, triggering senescence. Fi-

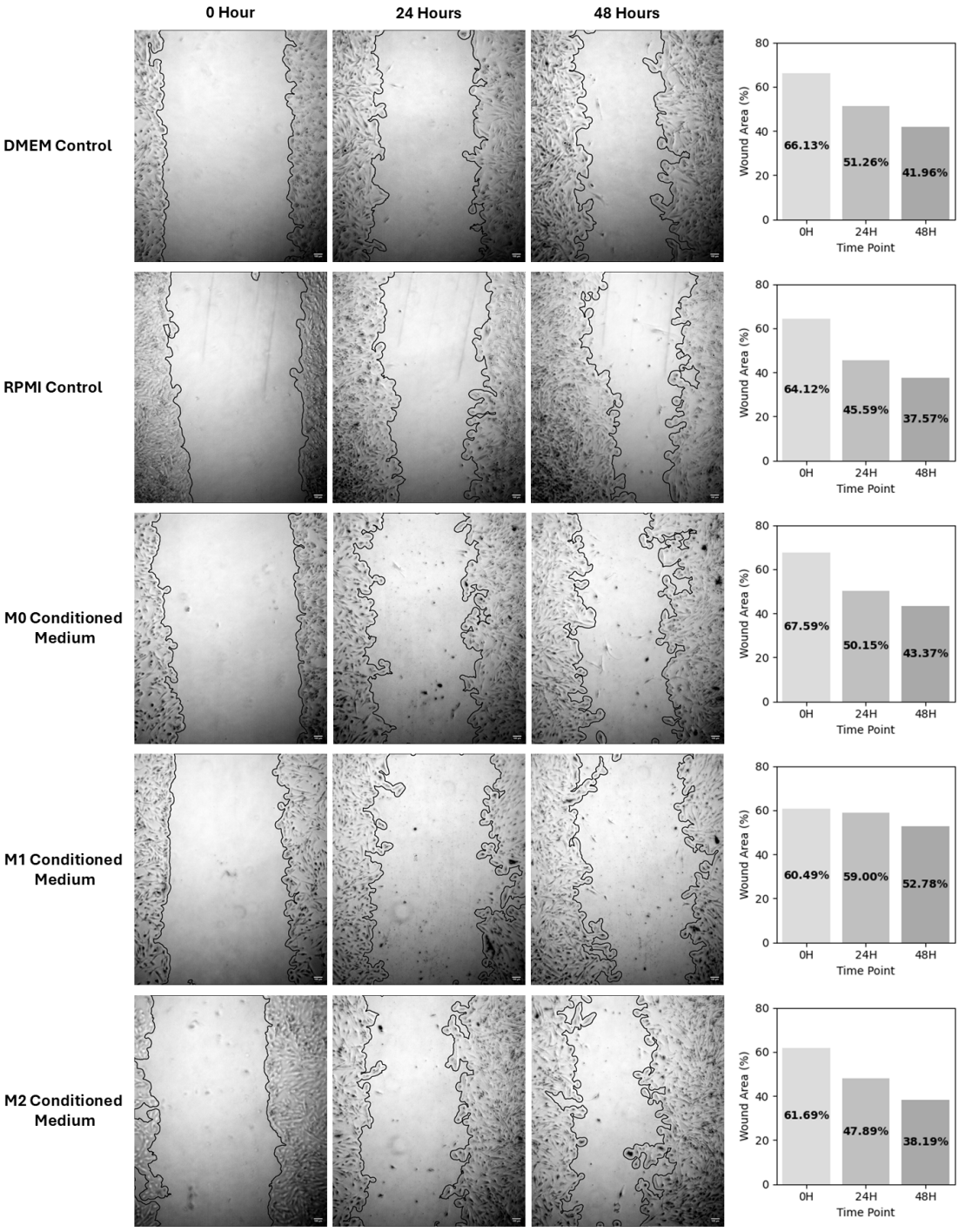

Figure 3.5 Analysed microscopic images of wound closure in different conditions via ImageJ software and wound area decrease. Images were captured at 4x. The scale bar for each image is 100 µm.

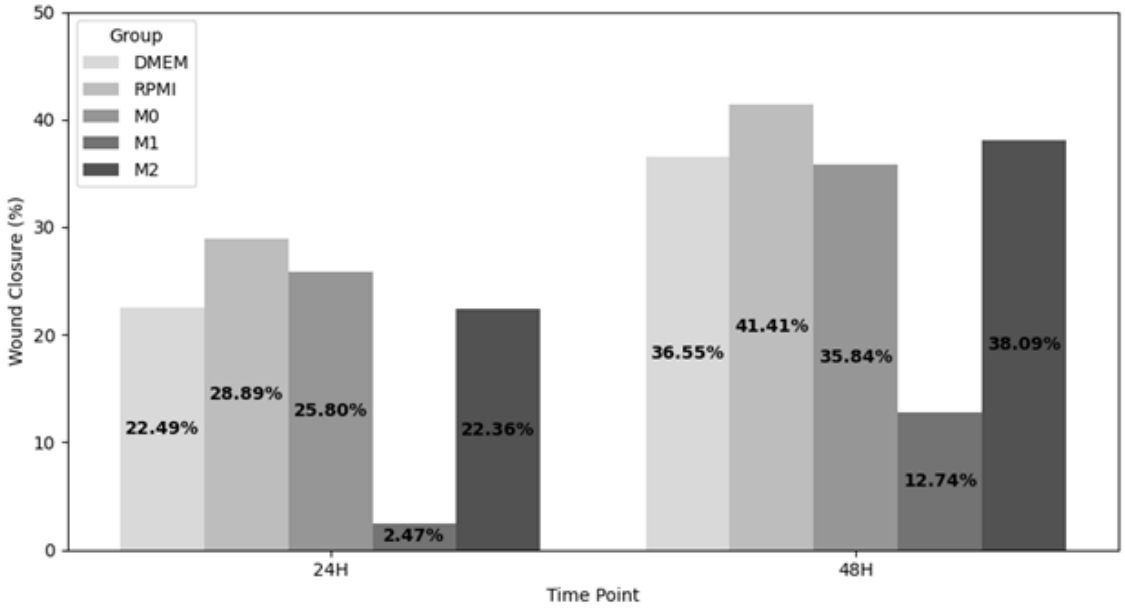

Figure 3.6 Wound closure percentage of U-87 cells grown in different conditioned media.

nally, these images can suggest that M0 macrophages and its soluble secreted factors show a modularity effect on glioma cell behavior resulting in phenotypic adaptations reflecting possible migration and early senescence. Acting on both migration and senescence can show the dual role of M0 macrophages. These findings highlight the complex role of unpolarized macrophages in the glioma microenvironment, suggesting that even in a non-polarized state, M0 macrophages and their secretome can induce adaptive phenotypic shifts in tumor cells that may contribute to disease progression or therapeutic resistance.

Additionally, U-87 and M0 macrophage co-culture did not show high morphological change compared to combined effect of both macrophages and conditioned media. It can be claimed that cytokines already secreted into media can elicit more rapid response compared to macrophages which first have to adapt themself to the environment before initiating any response against cancer.

Furthermore, contrary to the current dogma, glioma-associated myeloid cells (GAMs) showed distinct immunological functions, and Gabrusiewicz et al. (2016) proposed that they are more aligned with a non-polarized M0-like state rather than classical M1 or M2 polarization. This suggests that TAMs in GBM occupy a highly plastic and intermediate activation state, emphasizing the limitations of the traditional M1/M2 dichotomy in the context of tumor immunology.

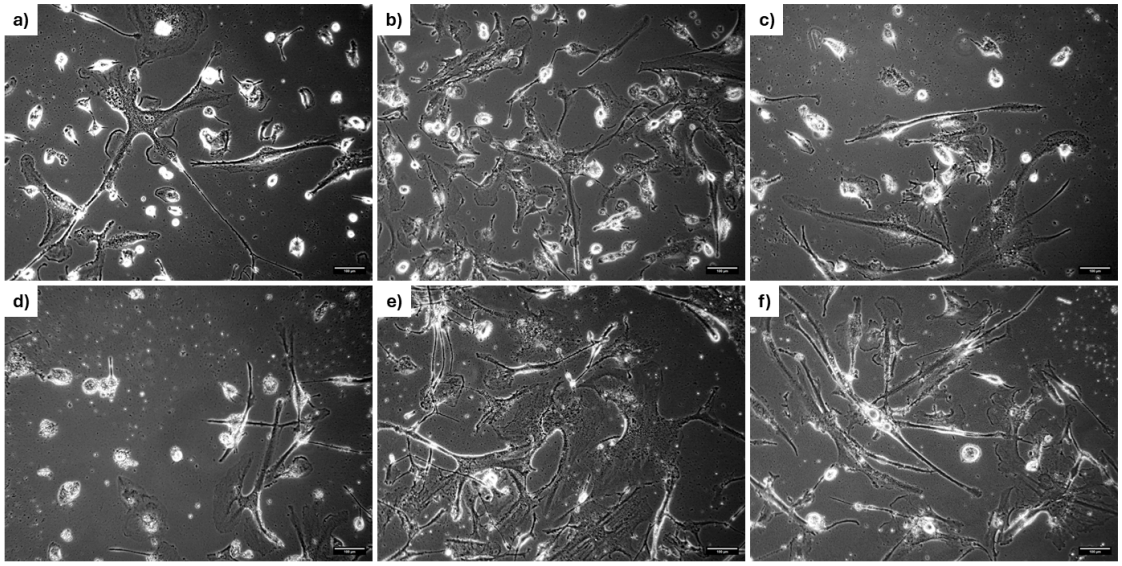

Figure 3.7 Morphological changes in U-87 cells co-cultured with M0 macrophages. In the presence of both M0 macrophages and their conditioned media, cells became flattened and longer, and expanded their cytoplasm after 48 hours (a), 72 hours (b), 96 hours (c), 120 hours (d), 144 hours (e) and U-87 cells under normal conditions (f). All images were captured at 10x. The scale bar for each image is 100 µm.

3.6 Simulation of Microfluidic Device

To investigate the hydrodynamic and electrical environment within a design microfluidic chip, the COMSOL Multiphysics simulation programme helps to simulate the electric field distribution and fluid flow behaviour. For computational simplicity in the simulation, an electrode array covering an area of 2 cm $\times$ 3 cm was used. In this model, the electrodes were designed as cylindrical structures with a height of 100 μm and a radius of 100 μm, consistent with the design dimensions, and the distance between adjacent electrodes was set to 200 (Figure 3.8a). In fabrication, our electrodes were coated with aluminum and its specific permeability and conductivity were applied into the programme.

In previous studies, the range of Vpp changes between 1 and 10, and frequency range is also between 10 kHz and 50 MHz (Çağlayan et al., 2020; Chan et al., 2019). In our simulation we stayed in the range of prior studies and we applied optimal 5 Vpp. It is proper to create strong field gradients and DEP forces to manipulate cells without resulting in electrothermal effects, electroporation and cell membrane rupture. Additionally, the DEP buffer used in our system is 20 μS/cm which is low conductive. Higher voltages at low conductivity can cause joule heating that increases temperature.

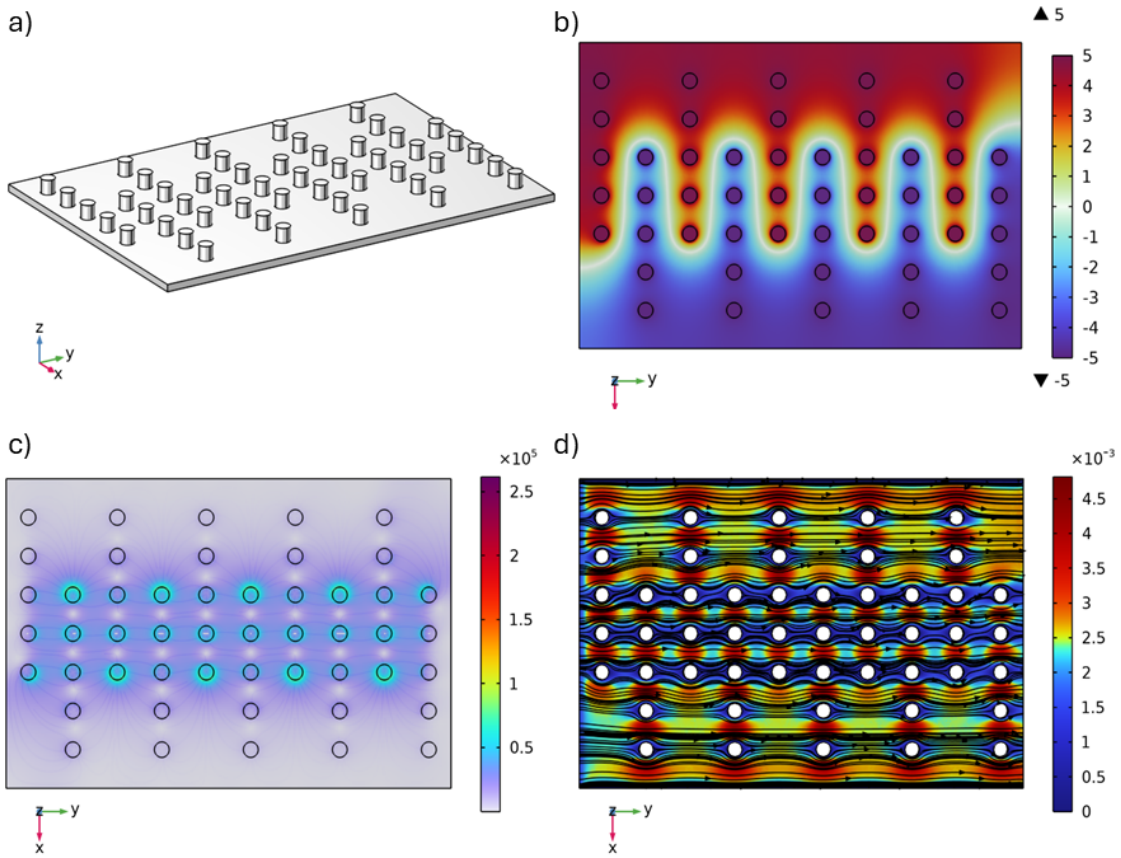

Figure 3.8 Comsol Multiphysics simulation of the microfluidic chip. Electrode arrangement in 3D (a), electric potential distribution between -5 Vpp and 5 Vpp across the electrode array (b), electric field intensity distribution at the electrode plane (c), velocity magnitude and streamlines of laminar flow inside the microfluidic channel, blue regions indicates low shear stress (d).

Figure 3.8b suggests that there is a well-formed voltage gradient between electrodes that supports generating non-uniform electric fields being essential for dielectrophoretic cell manipulation. Furthermore, the electric field intensity is concentrated close to electrode edges (Figure 3.8c). This indicates that the highest DEP force should be potentially in these regions. This spatial field distribution is beneficial for increased trapping efficiency of GBM cells via pDEP.

Figure 3.8d shows flow simulation of our chip. The blue color in this color map represents low flow velocity and areas where reduced shear stress is present while red color indicates higher velocity zones located in the central part of the electrodes. In the geometry, 3D electrodes disrupt the uniformity of the flow that forms localized low shear recirculation zones downstream of the electrodes. These reduced shear stress decreases the negative effects of DEP trapping on cells, like cell death and deformation. Together, these simulation results confirm that our chip design forms electrically and mechanically favorable microenvironment for trapping glioma cells via positive DEP force.

3.7 Viability of Cells in DEP Buffer

To demonstrate the effect of DEP buffer on U-87 cell viability, cells were counted before and after incubation in control DMEM and DEP buffer formulated with 20 μS/cm. Incubation time was 30 minutes, which is typical exposure time cells experience during DEP experiments on a chip. In Figure 3.9, there was no significant cell viability change between DMEM control and DEP buffer after 30 minutes of incubation. The cell viability of U-87 cells in DMEM media was slightly higher than in DEP buffer, but the p-value (0.7539) suggests that this result is not significant even if 3 replicates are present. Indeed, a 30-minute exposure to DEP buffer does not negatively affect U-87 cell viability.

This result is consistent with current literature that a low conductivity environment is safe for short term DEP based manipulation systems. We also preferred the low-conductivity buffer. The reason is that increased conductivity of the medium or buffer might cause death of cells or damage them because of joule heating, oxidative stress or electroporation (Sengul et al., 2024). Even this result suggests safe usage of DEP buffer for short term; the effect of long-term incubations, applying high frequency or higher voltage fields should be considered.

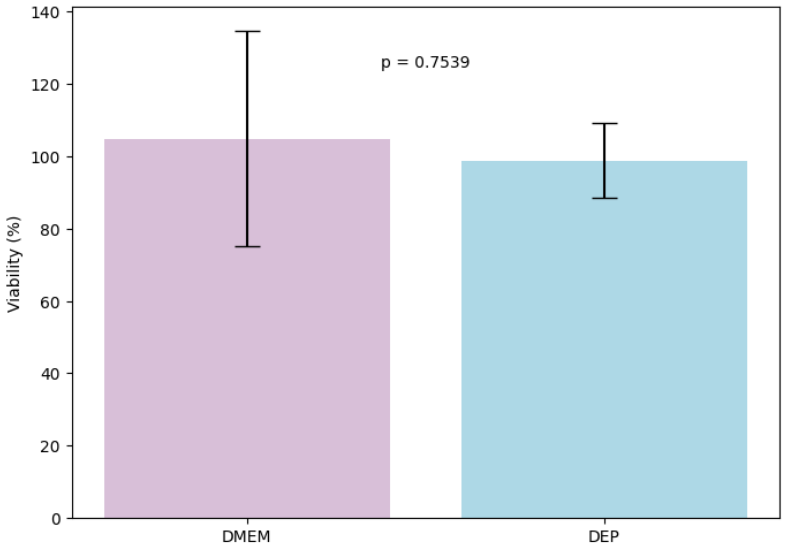

Figure 3.9 Mean cell viability of U-87 cells in DMEM media and DEP buffer after 30 minutes incubation. Sample size is 3 and p-value is 0.7539.

3.8 Empedans Measurements

To understand the electrical behaviour of U-87 and THP-1 cells on aluminum-coated 3D microfluidic chip, impedance spectroscopy was performed across a frequency range between 100 Hz to 1 MHz (Figure 3.10). To interpret values taken from spectroscopy and analyze differences, Nyquist, phase and magnitude based on frequency plots were generated. In Figure 3.10a, imaginary (Z'') impedance is related to capacitive/inductive components while real (Z') impedance shows resistive components. Therefore, the shape and pick point of each curve provide insights to analyze electrical properties of samples. Furthermore, there is a shift for each cell type in the impedance arc when they are added into the DEP buffer. This shows that there are changes in charge transfer and capacitive behavior at the electrode surface. The disruption of semicircular arc characteristics suggest increased complexity in the interface of electrode-electrolyte because of cell adhesion or membrane effects. Indeed, U-87 cells present high capacitance compared to THP-1 cells. In Figure 3.10c, decrease in impedance magnitude compared to DEP buffer control between 50 kHz and 900 kHz implies that cell suspension increases conductivity. Frequency dependent phase plot (Figure 3.10b) also shows the leading of phase which is corresponding to capacitive behavior. These two plots prove the Nyquist plot results with frequency values.

In the human body, biological systems work as complex electrical circuits containing resistive and capacitive elements. These decide how tissues respond to alternative

current and how impedance acts at different frequencies. Resistive behaviour is related to ion flow in cytoplasm, ECM and interstitial fluid. Therefore, resistance level is low in tissues containing more water and electrolytes. Additionally, the plasma membrane of a cell acts like a capacitor in this circuit. Lipid bilayer of membrane separates charges across it and membrane stores charges and shows delay in current flow. Current is not able to pass through where capacitance level is high generally at lower frequencies. At higher frequencies, capacitance level is decreased and the membrane becomes more permeable to electrical current (Gorbunov et al., 2019). Therefore, analyzing their electrical behavior is crucial for cell separation.

These findings suggest that U-87 cells exhibit greater dielectric complexity and size compared to THP-1 cells. Richter et al. (2014) found in their research that monocytes show lower capacitance level compared to microglia indicating their smaller membrane area. Conclude, our chip system is clearly working and able to represent different electrical behaviour of cell types in the presence of the electrical field. The frequency range of 50 kHz to 1 MHz will be applied into microfluidic systems to capture attraction of cells toward electrodes.

3.9 Microscopic Images of GBM Cells on Microfluidic Chip at Different Frequencies

To understand the frequency-based response of glioma cells under the alternating current AC electrical field, the chip system (Figure 2.5b) was connected to an oscilloscope and placed on the microscope stage. In every 30 seconds applied frequency level was increased, the general frequency range was between 0 kHz - 1 MHz. Figure 3.11 shows the sequential frames of cell distribution at each frequency step. Increasing frequency resulted in notable changes in cell organization.

At 0 kHz, cells were randomly dispersed without any directional movement. Between 100-200 kHz, cells started to migrate and to align within the inter electrode region. After 400 kHz, cells formed clear chains, and other cells were attracted to these chains which form bridges between two electrode lines. These chain structures are defined as “pearl chains” that are oriented along the electrical field line (Sancho et al., 2010). The electrical field line can be seen in simulation results. The formation of chains is the result of induced dipole-dipole interactions between polarized cells. Once one cell is polarized on an electrode line, it experiences DEP force and generates

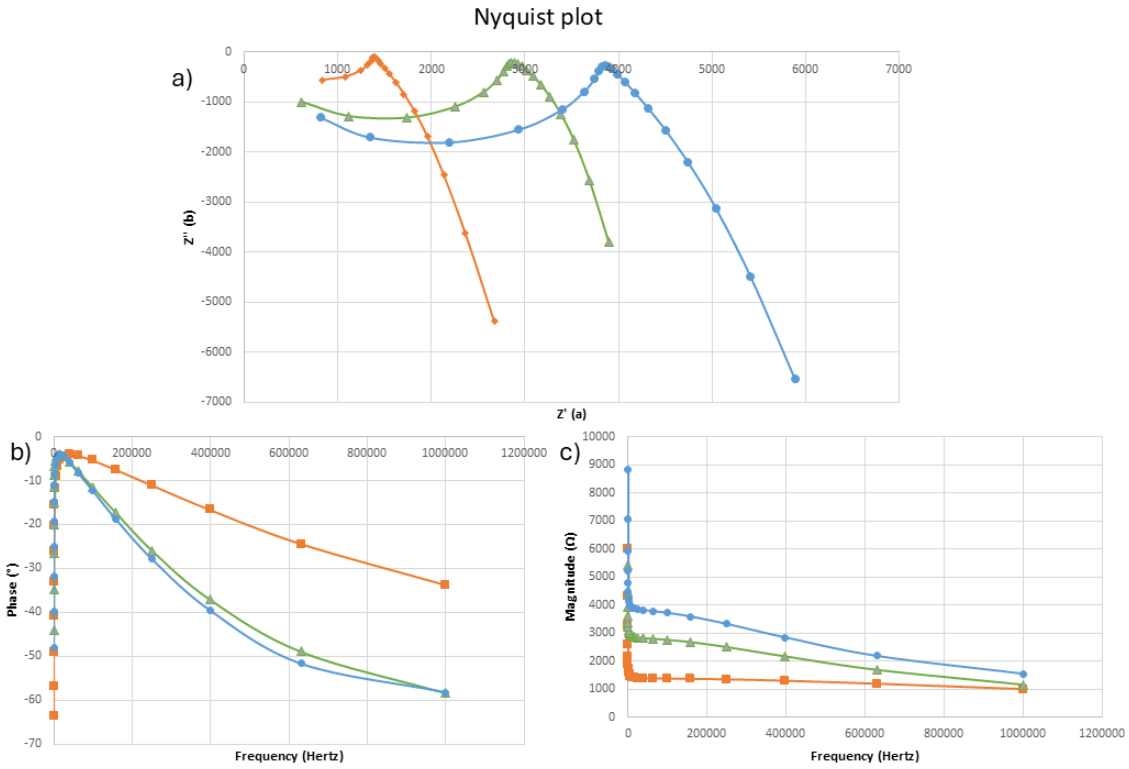

Figure 3.10 Impedance analysis of U-87 and THP-1 cells in DEP buffer on Al coated microfluidic chip. Nyquist plot showing the real (Z') and imaginary (Z'') components of impedance across frequency sweep (a), Phase angle vs. frequency plot that indicates resistive and capacitive behaviour of system in different conditions (b), Bode magnitude plot that shows total impedance magnitude over a 100 Hz to 1 MHz frequency range (c). Blue lines represent values for the DEP buffer while orange and green lines represent U-87 and THP-1 cells in the DEP buffer, respectively.

its own field.

The observed behaviour suggests that there is an attraction between cell-cell and cell-electrode line that aligns with the previous impedance change because of the change in capacitance level of cells. Sengul et al. (2024) suggests that U-87 cells can exhibit crossover frequency between 100-150 kHz, and cells can experience pDEP in different ranges (500 kHz to 10 MHz) suggesting morphologic heterogeneity of glioma cells. Similar to literature, our results showed an increase in trapping efficiency and formation of chains in this frequency range that suggests optimal cell attraction and manipulation.

Moreover, there is no direct nDEP and pDEP behaviour in our chip system. This is preliminary data to be able to understand our chip mechanism and its weakness to improve it. There should be some improvement. Masking electrode lines with photoresist may help to see only the effect of 3D electrodes field gradients. The current images are allowed to observe cells in 2D even though our chip system is 3D. Therefore, it is not possible to see how cells act along the vertical walls of 3D electrodes. Cells could be shown interaction or accumulation on sidewalls of electrons. There should be integration of 3D imaging system to provide comprehensive insights into interactions.

These observations illustrate that fabricated microfluidic chip systems are useful to produce stable and frequency dependent DEP responses in glioma cells. Visible changes in cell alignment and chain formation confirms that there is non-uniform electric field for cell manipulation. This chip system can serve; reliable real time visualization of cell responses to field, a platform to study glioma heterogeneity, and most importantly possible future diagnostic and therapeutic microfluidic systems.

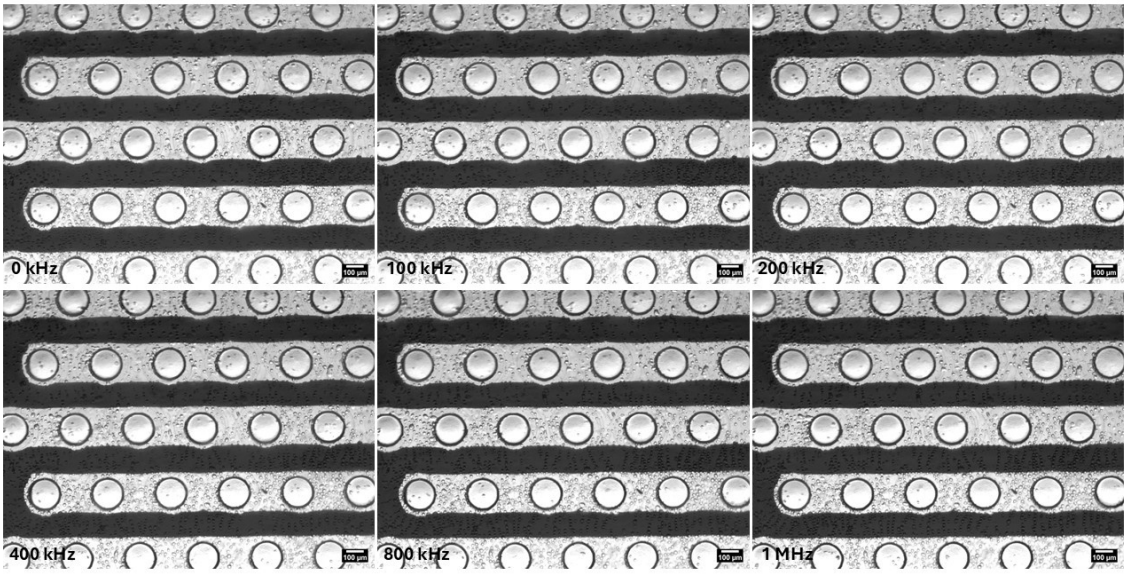

Figure 3.11 Microscopic images of U-87 glioma cells exposed to electric fields across a range of frequencies on 3D microfluidic chip.

4. CONCLUSION

In this thesis, the dual role of monocyte-derived macrophages in modulating the behaviour of GBM cells based on proliferation and migration was investigated, and a microfluidic chip system using DEP technique was explored to develop label-free cell separation tool for glioma cell analysis. Firstly, our results showed that THP-1 cells were triggered to differentiate in the presence of glioma cell conditioned media, which demonstrates that soluble factors released from tumor cells direct monocytes to differentiate into macrophages that function in the tumor microenvironment. Additionally, different polarization states of in-vitro differentiated macrophages (M0, M1, and M2) resulted in distinct effects on proliferation and migration of glioma cells. Soluble factors from M1 macrophages enhanced proliferation while a biphasic effect was observed in the case of M2, initially suppressing glioma cell growth but later promoting proliferation. In terms of migration capability, M1 macrophages showed a decrease compared to both M0 and M2 (Figure 3.6). Furthermore, glioma cells displayed noticeable morphological differences such as cytoplasmic expansion correlated with early senescence, when grown in the presence of M0 macrophages and conditioned media. These findings emphasize the high plasticity of polarized macrophages and highlight the importance of understanding complex tumor-immune interactions that facilitate glioblastoma heterogeneity.

In parallel, a 3D aluminum coated microfluidic chip was designed and fabricated to provide a non-uniform electrical field for dielectrophoresis and enable frequency dependent manipulation of GBM cells. Impedance spectroscopy results confirmed that different cell types were affected individually by the same frequency reflecting membrane potential characteristics of cells. Additionally, microscope images of glioma cells at several frequencies showed cell alignment and pearl chain formation supporting the functionality of our chip in cell manipulation. Importantly, DEP buffer preserved the viability of glioma cells that validates its suitability for short term and non-destructive applications. These results confirm the potential use of this tool to characterize electrical properties and heterogeneity of glioma cells.

To conclude, this thesis enhances our knowledge on glioblastoma research by rep-

resenting the different effects of macrophage subtypes on cell proliferation and migration, and introduces the initial promise of DEP-integrated microfluidic chips which can be further used for glioma diagnosis and therapeutic approaches. Future research should focus on identifying the specific soluble factors that mediate macrophage-glioma interactions, integrating DEP analyses with single cell profiling, and developing cell separation using closed-channel metal-coated chips. Furthermore, patient derived samples can be tested for diagnostic purposes. This work combines biological insights with engineering innovations, and provides a foundation for more precise diagnostic aspects and therapeutic interventions against this highly aggressive brain tumor.

BIBLIOGRAPHY

Adekanmbi, E. O. & Srivastava, S. K. (2016). Dielectrophoretic applications for disease diagnostics using lab-on-a-chip platforms. *Lab on a Chip*, *16*(12), 2148–2167.

Andersen, R. S., Anand, A., Harwood, D. S. L., & Kristensen, B. W. (2021). Tumor-Associated microglia and macrophages in the glioblastoma microenvironment and their implications for therapy. *Cancers*, *13*(17), 4255.

Atajanov, A., Zhbanov, A., & Yang, S. (2018). Sorting and manipulation of biological cells and the prospects for using optical forces. *Micro and Nano Systems Letters*, *6*(1).

Baxter, E., Graham, A., Re, N., Carr, I., Robinson, J., Mackie, S., & Morgan, A. (2020). Standardized protocols for differentiation of THP-1 cells to macrophages with distinct M(IFNγ+LPS), M(IL-4) and M(IL-10) phenotypes. *Journal of Immunological Methods*, *478*, 112721.

Beck, J., Horikawa, I., & Harris, C. (2020). Cellular senescence: mechanisms, morphology, and mouse models. *Veterinary Pathology*, *57*(6), 747–757.

Bellail, A. C., Hunter, S. B., Brat, D. J., Tan, C., & Van Meir, E. G. (2004). Microregional extracellular matrix heterogeneity in brain modulates glioma cell invasion. *The International Journal of Biochemistry & Cell Biology*, *36*(6), 1046–1069.

Bikfalvi, A., Da Costa, C. A., Avril, T., Barnier, J.-V., Bauchet, L., Brisson, L., Cartron, P. F., Castel, H., Chevet, E., Chneiweiss, H., Clavreul, A., Constantin, B., Coronas, V., Daubon, T., Dontenwill, M., Ducray, F., Entz-Werlé, N., Figarella-Branger, D., Fournier, I., Frenel, J.-S., Gabut, M., Galli, T., Gavard, J., Huberfeld, G., Hugnot, J.-P., Idbaih, A., Junier, M.-P., Mathivet, T., Menei, P., Meyronet, D., Mirjolet, C., Morin, F., Mosser, J., Moyal, E. C.-J., Rousseau, V., Salzet, M., Sanson, M., Seano, G., Tabouret, E., Tchoghandjian, A., Turchi, L., Vallette, F. M., Vats, S., Verreault, M., & Virolle, T. (2022). Challenges in glioblastoma research: focus on the tumor microenvironment. *Trends in cancer*, *9*(1), 9–27.

Buonfiglioli, A. & Hambardzumyan, D. (2021). Macrophages and microglia: the cerberus of glioblastoma. *Acta Neuropathologica Communications*, *9*(1).

Chan, J. Y., Kayani, A. B. A., Ali, M. A. M., Kok, C. K., Buyong, M. R., Hoe, S. L. L., Marzuki, M., Khoo, A. S., Sriram, S., & Ostrikov, K. (2019). Dielectrophoretic deformation of breast cancer cells for lab on a chip applications. *Electrophoresis*, *40*(20), 2728–2735.

Chen, P., Hsu, W.-H., Han, J., Xia, Y., & DePinho, R. A. (2021). Cancer stemness meets immunity: From mechanism to therapy. *Cell Reports*, *34*(1), 108597.

Chen, Y., Song, Y., Du, W., Gong, L., Chang, H., & Zou, Z. (2019). Tumor-associated macrophages: an accomplice in solid tumor progression. *Journal of Biomedical Science*, *26*(1).

Chowdhury, P., Talukdar, P. D., Mukherjee, P., Dey, D., Chatterji, U., & Sengupta, S. (2024). Hemin-induced reactive oxygen species triggers autophagy-dependent macrophage differentiation and pro-inflammatory responses in THP-1 cells. *Experimental Cell Research*, *442*(1), 114216.

Eisenbarth, D. & Wang, Y. A. (2023). Glioblastoma heterogeneity at single cell resolution. *Oncogene*, *42*(27), 2155–2165.

Erices, J. I., Bizama, C., Niechi, I., Uribe, D., Rosales, A., Fabres, K., Navarro-Martínez, G., Torres, , Martín, R. S., Roa, J. C., & Quezada-Monrás, C. (2023). Glioblastoma Microenvironment and invasiveness: New insights and therapeutic targets. *International Journal of Molecular Sciences*, *24*(8), 7047.

Fan, J., Schiemer, T., Vaska, A., Jahed, V., & Klavins, K. (2024). Cell via Cell Viability Assay Changes Cellular Metabolic Characteristics by Intervening with Glycolysis and Pentose Phosphate Pathway. *Chemical Research in Toxicology*, *37*(2), 208–211.

Fornell, A., Cushing, K., Nilsson, J., & Tenje, M. (2018). Binary particle separation in droplet microfluidics using acoustophoresis. *Applied Physics Letters*, *112*(6).

Gabrusiewicz, K., Rodriguez, B., Wei, J., Hashimoto, Y., Healy, L. M., Maiti, S. N., Thomas, G., Zhou, S., Wang, Q., Elakkad, A., Liebelt, B. D., Yaghi, N. K., Ezhilarasan, R., Huang, N., Weinberg, J. S., Prabhu, S. S., Rao, G., Sawaya, R., Langford, L. A., Bruner, J. M., Fuller, G. N., Bar-Or, A., Li, W., Colen, R. R., Curran, M. A., Bhat, K. P., Antel, J. P., Cooper, L. J., Sulman, E. P., & Heimberger, A. B. (2016). Glioblastoma-infiltrated innate immune cells resemble M0 macrophage phenotype. *JCI Insight*, *1*(2).

Giduthuri, A. T., Theodossiou, S. K., Schiele, N. R., & Srivastava, S. K. (2020). Dielectrophoresis as a tool for electrophysiological characterization of stem cells. *Biophysics Reviews*, *1*(1).

Gieryng, A., Pszczolkowska, D., Walentynowicz, K. A., Rajan, W. D., & Kaminska, B. (2017). Immune microenvironment of gliomas. *Laboratory Investigation*, *97*(5), 498–518.

Gopinath, V. K., Soumya, S., & Mohammad, M. G. (2020). Ror β expression in activated macrophages and dental pulp stem cells. *International Endodontic Journal*, *54*(3), 388–398.

Gorbunov, A., Gromov, Y., & Egorov, V. (2019). The calculation of the impedance of biological tissue on the model of Yamamoto in the process of galvanic effects. *Journal of Physics Conference Series*, *1278*(1), 012037.

Gordon, S. (2003). Alternative activation of macrophages. *Nature reviews. Immunology*, *3*(1), 23–35.

Gossett, D. R., Weaver, W. M., Mach, A. J., Hur, S. C., Tse, H. T. K., Lee, W., Amini, H., & Di Carlo, D. (2010). Label-free cell separation and sorting in microfluidic systems. *Analytical and Bioanalytical Chemistry*, *397*(8), 3249–3267.

Gough, R., Treffy, R. W., Krucoff, M. O., & Desai, R. (2025). Advances in glioblastoma diagnosis: integrating genetics, noninvasive sampling, and advanced imaging. *Cancers*, *17*(1), 124.

Hawkins, B. G., Lai, N., & Clague, D. S. (2020). High-Sensitivity in dielectrophoresis separations. *Micromachines*, *11*(4), 391.

Hegi, M. E., Diserens, A.-C., Gorlia, T., Hamou, M.-F., De Tribolet, N., Weller, M., Kros, J. M., Hainfellner, J. A., Mason, W., Mariani, L., Bromberg, J. E., Hau, P., Mirimanoff, R. O., Cairncross, J. G., Janzer, R. C., & Stupp, R. (2005). MGMTGene Silencing and Benefit from Temozolomide in Glioblastoma. *New England Journal of Medicine*, *352*(10), 997–1003.

Hejazian, M., Li, W., & Nguyen, N.-T. (2014). Lab on a chip for continuous-flow magnetic cell separation. *Lab on a Chip*, *15*(4), 959–970.

Henslee, E. A. (2020). Review: Dielectrophoresis in cell characterization. *Electrophoresis*, *41*(21-22), 1915–1930.

Hosseini, A., Ashraf, H., Rahimi, F., Alipourfard, I., Alivirdiloo, V., Hashemi, B., Yazdani, Y., Ghazi, F., Eslami, M., Reza, M. A. S., & Dadashpour, M. (2023). Recent advances in the detection of glioblastoma, from imaging-based methods to proteomics and biosensors: A narrative review. *Cancer Cell International*, *23*(1).

Jiang, A. Y. L., Yale, A. R., Aghaamoo, M., Lee, D.-H., Lee, A. P., Adams, T. N. G., & Flanagan, L. A. (2019). High-throughput continuous dielectrophoretic separation of neural stem cells. *Biomicrofluidics*, *13*(6).

Khan, F., Pang, L., Dunterman, M., Lesniak, M. S., Heimberger, A. B., & Chen, P. (2023). Macrophages and microglia in glioblastoma: heterogeneity, plasticity, and therapy. *Journal of Clinical Investigation*, *133*(1).

Lee, S. J., Kang, W. Y., Yoon, Y., Jin, J. Y., Song, H. J., Her, J. H., Kang, S. M., Hwang, Y. K., Kang, K. J., Joo, K. M., & Nam, D.-H. (2015). Natural killer (NK) cells inhibit systemic metastasis of glioblastoma cells and have therapeutic effects against glioblastomas in the brain. *BMC Cancer*, *15*(1).

Lenshof, A. & Laurell, T. (2010). Continuous separation of cells and particles in microfluidic systems. *Chemical Society Reviews*, *39*(3), 1203.

Liu, T., Huang, T., Li, J., Li, A., Li, C., Huang, X., Li, D., Wang, S., & Liang, M. (2023). Optimization of differentiation and transcriptomic profile of THP-1 cells into macrophage by PMA. *PLoS ONE*, *18*(7), e0286056.

Lomovskaya, Y. V., Kobyakova, M. I., Senotov, A. S., Lomovsky, A. I., Minaychev, V. V., Fadeeva, I. S., Shtatnova, D. Y., Krasnov, K. S., Zvyagina, A. I., Akatov, V. S., & Fadeev, R. S. (2022). Macrophage-like THP-1 Cells Derived from High-Density Cell Culture Are Resistant to TRAIL-Induced Cell Death via Down-Regulation of Death-Receptors DR4 and DR5. *Biomolecules*, *12*(2), 150.

Louis, D. N., Perry, A., Wesseling, P., Brat, D. J., Cree, I. A., Figarella-Branger, D., Hawkins, C., Ng, H. K., Pfister, S. M., Reifenberger, G., Soffietti, R., Von Deimling, A., & Ellison, D. W. (2021). The 2021 WHO Classification of Tumors of the Central Nervous System: a summary. *Neuro-Oncology*, *23*(8), 1231–1251.

Mahmoudian, M., Trotta, F., Raimondo, S., Bussolino, F., & Arese, M. (2025). Cell Membrane-Integrated neuroligin-1 regulates the Anti-Inflammatory effects of CRC Cell-Derived exosomes. *International Journal of Molecular Sciences*, *26*(2), 503.

Maidin, N. N. M., Buyong, M. R., Rahim, R. A., & Mohamed, M. A. (2021). Dielectrophoresis applications in biomedical field and future perspectives in biomedical technology. *Electrophoresis*, *42*(20), 2033–2059.

Marino, S., Menna, G., Di Bonaventura, R., Lisi, L., Mattogno, P., Figà, F., Bilgin, L., D'Alessandris, Q. G., Olivi, A., & Della Pepa, G. M. (2023). The extracellular matrix in glioblastomas: A glance at its structural modifications in shaping the Tumoral Microenvironment—A Systematic Review. *Cancers*, *15*(6), 1879.

Nasiri, R., Shamloo, A., Ahadian, S., Amirifar, L., Akbari, J., Goudie, M. J., Lee,

K., Ashammakhi, N., Dokmeci, M. R., Di Carlo, D., & Khademhosseini, A. (2020). Microfluidic-Based Approaches in Targeted Cell/Particle Separation Based on Physical Properties: Fundamentals and applications. *Small*, *16*(29).

Parmigiani, E., Scalera, M., Mori, E., Tantillo, E., & Vannini, E. (2021). Old stars and new players in the brain tumor microenvironment. *Frontiers in Cellular Neuroscience*, *15*.

Picot, J., Guerin, C. L., Van Kim, C. L., & Boulanger, C. M. (2012). Flow cytometry: retrospective, fundamentals and recent instrumentation. *Cytotechnology*, *64*(2), 109–130.

Read, R. D., Tapp, Z. M., Rajappa, P., & Hambardzumyan, D. (2024). Glioblastoma microenvironment—from biology to therapy. *Genes & Development*.

Ribeiro, A. R. B., Silva, E. C. O., Araújo, P. M. C., Souza, S. T., Da Silva Fonseca, E. J., & Barreto, E. (2021). Application of Raman spectroscopy for characterization of the functional polarization of macrophages into M1 and M2 cells. *Spectrochimica Acta Part A Molecular and Biomolecular Spectroscopy*, *265*, 120328.

Richter, N., Wendt, S., Georgieva, P. B., Hambardzumyan, D., Nolte, C., & Kettenmann, H. (2014). Glioma-associated microglia and macrophages/monocytes display distinct electrophysiological properties and do not communicate via gap junctions. *Neuroscience Letters*, *583*, 130–135.

Sancho, M., Martínez, G., Muñoz, S., Sebastián, J. L., & Pethig, R. (2010). Interaction between cells in dielectrophoresis and electrorotation experiments. *Biomicrofluidics*, *4*(2).

Sarno, B., Heineck, D., Heller, M. J., & Ibsen, S. D. (2020). Dielectrophoresis: Developments and applications from 2010 to 2020. *Electrophoresis*, *42*(5), 539–564.

Sengul, E., Sharbati, P., Islam, M., Korvink, J., & Elitas, M. (2024). Dielectrophoretic spectra of glioma U87 cells using a microfluidic gold electrode array. *Authorea (Authorea)*.

Sisakht, A. K., Malekan, M., Ghobadinezhad, F., Firouzabadi, S. N. M., Jafari, A., Mirazimi, S. M. A., Abadi, B., Shafabakhsh, R., & Mirzaei, H. (2022). Cellular conversations in glioblastoma Progression, diagnosis and treatment. *Cellular and Molecular Neurobiology*, *43*(2), 585–603.

Solomou, G., Young, A. M. H., & Bulstrode, H. J. C. J. (2024). Microglia and macrophages in glioblastoma: landscapes and treatment directions. *Molecular Oncology*.

Strepkos, D., Markouli, M., Klonou, A., Piperi, C., & Papavassiliou, A. G. (2019). Insights in the immunobiology of glioblastoma. *Journal of Molecular Medicine*, *98*(1), 1–10.

Sun, H.-J., Chen, J., Ni, B., Yang, X., & Wu, Y.-Z. (2015). Recent advances and current issues in single-cell sequencing of tumors. *Cancer Letters*, *365*(1), 1–10.

Sun, Y.-S. (2016). Comparison of chip inlet geometry in microfluidic devices for cell studies. *Molecules*, *21*(6), 778.

Sørensen, M. D., Dahlrot, R. H., Boldt, H. B., Hansen, S., & Kristensen, B. W. (2017). Tumour-associated microglia/macrophages predict poor prognosis in high-grade gliomas and correlate with an aggressive tumour subtype. *Neuropathology and Applied Neurobiology*, *44*(2), 185–206.

Wang, F., Liao, W., Li, C., & Zhu, L. (2024). Silencing BMAL1 promotes M1/M2 polarization through the LDHA/lactate axis to promote GBM sensitivity to bevacizumab. *International Immunopharmacology*, *134*, 112187.

Wang, G., Zhong, K., Wang, Z., Zhang, Z., Tang, X., Tong, A., & Zhou, L. (2022). Tumor-associated microglia and macrophages in glioblastoma: From basic insights to therapeutic opportunities. *Frontiers in Immunology*, *13*.

Yang, L., Fang, J., & Chen, J. (2017). Tumor cell senescence response produces aggressive variants. *Cell Death Discovery*, *3*(1).

Zhang, H., Chang, H., & Neuzil, P. (2019). DEP-on-a-Chip: Dielectrophoresis applied to microfluidic platforms. *Micromachines*, *10*(6), 423.

Zottel, A., Jovčevska, I., & Šamec, N. (2023). Non-animal glioblastoma models for personalized treatment. *Heliyon*, *9*(10), e21070.

Çağlayan, Z., Yalçın, Y. D., & Külah, H. (2020). Examination of the dielectrophoretic spectra of MCF7 breast cancer cells and leukocytes. *Electrophoresis*, *41*(5-6), 345–352.

Șovrea, A. S., Boșca, B., Melincovici, C. S., Constantin, A.-M., Crintea, A., Mărginean, M., Dronca, E., Jianu, M. E., Suflețel, R., Gonciar, D., Bungărdean, M., & Crivii, C.-B. (2022). Multiple faces of the glioblastoma microenvironment. *International Journal of Molecular Sciences*, *23*(2), 595.